Plant Stress 21 (2026) 101434

Contents lists available at ScienceDirect

Plant Stress

journal homepage: www.sciencedirect.com/journal/plant-stress

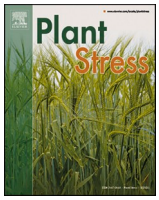

Beneficial bacteria and arbuscular mycorrhizal fungi mitigate Cd+Zn stress in tomato through coordinated changes in ion homeostasis, root exudation and rhizosphere microbiome structure

Leilei Zhang [a,*], Monica Yorlady Alzate Zuluaga [b], Gabriele Bellotti [a], Hajar Salehi [a], Angelica Barone [c], Filippo Vaccari [a], Stefano Amaducci [c], Youry Pii [b], Edoardo Puglisi [a], Luigi Lucini [a]

[a] Department for Sustainable Food Process, Università Cattolica del Sacro Cuore, Piacenza, Italy
[b] Faculty of Science and Technology, Free University of Bozen-Bolzano, Bolzano, Italy
[c] Department of Sustainable Crop Production, Università Cattolica del Sacro Cuore, Piacenza, Italy

ARTICLE INFO

Keywords:
Heavy metal stress
Bioremediation
Microbial biostimulants
Multi-omics integration
Rhizosphere microbiome

ABSTRACT

Heavy metal (HM) pollution from agricultural practices accumulates in soils, moving through crops and food chains, posing significant environmental concerns that threaten ecosystem integrity and human health. In this study, the morphophysiological traits e.g., biomass, relative water content, membrane stability, PSII efficiency and oxidative stress markers, as well as the allocation of metals and nutrients in different plant tissues, and the changes in the root microbiota are assessed in tomato plants exposed to combined Cd+Zn stress and inoculated with two microbial biostimulants (MB): a plant growth-promoting rhizobacterium (PGPR) and an arbuscular mycorrhiza (AMF) consortium. Cd+Zn exposure affected morphophysiological traits, reducing shoot and root biomass (12% and 9.5%, respectively) and membrane stability by 37.7% in tomatoes, and reshaped root exudation patterns, but MBs improved tomato resilience by mitigating these effects. AMF improved root development and metabolite accumulation with antioxidant, membrane-protective, and metal-chelating functions. PGPR effectively restored shoot fresh and dry biomass, reduced leaf ROS accumulation, and limited Cd accumulation across tomato organs. Specifically, it induced more complex metabolic reprogramming, reducing lipid and phenolic turnover while accumulating steroidal saponins and N-containing compounds. At the rhizosphere level, PGPR significantly increased bacterial and fungal richness relative to the control (Chao1, $p < 0.01$ and $p < 0.05$, respectively). Multi-omics integration further showed strong metabolite–microbiome associations ($r > |0.9|$), with PGPR treatment enriching fungal families (e.g., Aspergillaceae and Chaetomiaceae) and bacterial orders (e.g., Flavobacteriales and Rhizobiales), which were positively correlated with root exudates and potentially involved in organic matter turnover, nutrient cycling, and HM detoxification.

Introduction

Heavy metal (HM) contamination is a significant environmental concern that threatens ecosystem integrity and human health. In agricultural soils, intensive farming practices can promote the accumulation of HMs and other pollutants through long-term inputs such as fertilizers, pesticides, manure, and contaminated irrigation water. This contamination can impair soil health and crop productivity, facilitate the transfer of pollutants to plants and groundwater, and ultimately increase risks along the food chain (Rashid et al., 2023). In most plants, HMs, such as lead (Pb), cadmium (Cd), arsenic (As), zinc (Zn), copper (Cu), and other metals, are taken up by roots via intermembrane transporters shared with essential elements and can also be absorbed directly into the leaves due to particle deposition on the leaf surfaces. The accumulation of HMs in plants not only affects plant performance but also causes serious health problems that amplify through the food chain (Sharafi and Salehi, 2025). The mechanisms by which HMs disturb biochemical, metabolic, and physiological processes in plants include the disruption of nutrient uptake, induction of oxidative stress, reduction of antioxidant activity, and aggravation of ultrastructural damage to plant

* Corresponding author.
E-mail address: leilei.zhang@unicatt.it (L. Zhang).

https://doi.org/10.1016/j.stress.2026.101434
Received 19 January 2026; Received in revised form 21 May 2026; Accepted 30 May 2026
Available online 1 June 2026

cells (Angulo-Bejarano et al., 2021; Balali-Mood et al., 2021; Dutta et al., 2018).

In recent studies, a single application of HM has been reported to be sufficient to induce toxicity in various plants, depending on factors such as plant species, phenological growth stage, and soil physicochemical properties (Alengebawy et al., 2021). On the other hand, the co-exposure of multiple HMs in plants may induce either synergistic, antagonistic, or additive effects that increase or reduce toxicity (Kiran et al., 2022; Lanier et al., 2019; Sperdouli, 2022). Furthermore, plant responses cannot be fully understood by considering growth and physiology alone, because HM stress also reshapes belowground biochemical interactions and mineral allocation patterns (Jarin et al., 2025). Notably, root exudation is central to plant adaptation to stress, as it releases a complex mixture of amino acids, sugars, organic acids, phenolics, coumarins, lipids, and other specialized metabolites that regulate nutrient mobilization, metal complexation, and rhizosphere signaling (Jarin et al., 2025). Under HM stress, these exudation patterns may shift markedly, reflecting both plant defense responses and the selective recruitment of beneficial microorganisms (Jarin et al., 2025). Specifically, metagenomics enables the characterization of bacterial and fungal taxa responsive to stress and inoculation, providing insight into microbial shifts associated with nutrient cycling, organic matter turnover, and detoxification-related functions (Galanova et al., 2025). Increasing evidence suggests that PGPR and AMF can modify rhizosphere communities not only through direct inoculation effects but also by altering the exudate environment, thereby selecting specific microbial groups (Kong and Liu, 2022). In this regard, plant-microbe communication under HM stress via root exudates is fundamental for understanding the belowground mechanism of action, and the application of targeted chemometric approaches, including multi-omics dataset integration, can provide deeper insight into these complex interactions (L. Zhang et al., 2025).

Reducing and alleviating the side effects of HMs has become a challenging task. To mitigate their impacts on soils, three categories have been proposed, including chemical, physicochemical, and biological methods. Among biological strategies proposed for HM-contaminated agricultural soils, two approaches should be considered: remediation, which removes contaminants from soil, and mitigation, which reduces their bioavailability, phytotoxicity, and transfer to the food chain. In the current context, microbial biostimulants may represent a promising mitigation tool, as they can alleviate metal-induced stress in plants and influence rhizosphere processes that decrease metal mobility and bioavailability through microbially mediated processes, including biosorption, complexation, precipitation, and the secretion of extracellular compounds to immobilize, transform, or detoxify contaminants (Kaushal and Pati, 2025; Tamma et al., 2025). As a result, these treatments may reduce heavy metal uptake by crops while improving plant performance and soil biological functioning. Various bacterial and fungal species have been reported to actively metabolize and decrease the absorption and subsequently the toxicity of HMs (Gaur et al., 2021). Plant growth-promoting rhizobacterium (PGPR) and arbuscular mycorrhiza fungi (AMF) were reported to have great potential in the bioremediation of HMs-contaminated soils (Chen et al., 2023). PGPRs can facilitate detoxification mainly by synthesizing metal-chelating molecules that dilute metal concentrations in plant tissues. Furthermore, PGPRs improve the nutrient uptake and induce HM tolerance in plants (Syed et al., 2023). AMF contribute to the symbiotic relationship with plant roots by developing specialized structures defined as “arbuscules” in root cells. Arbuscules are involved in enhancing nutrient uptake (particularly phosphorus and nitrogen) and water absorption (Rajapitamahuni et al., 2023). Furthermore, this mycorrhizal-root interaction can decrease the uptake of toxic metals and improve the resistance to HMs-induced stress (Riaz et al., 2021). For example, Rask et al. (2019) reported that moderate levels of Cd stimulated mycorrhizal colonisation in *Hordeum vulgare* and, as a result, this symbiosis reduced Cd translocation from roots to shoots (Rask et al., 2019). The study also reported that the high Cd avoidance seems to be due to strong root retention, which keeps the Cd within the root system away from the upper parts of the plant. Although both PGPR and AMF have shown potential in alleviating HM toxicity, optimal applications depend on the specific HM, exposure, and association with the target plant, making the results difficult to predict. Our most recent studies provide strong indications that the application of two specific MBs not only improved the physiological process of tomato plants grown in soil polluted with Zn or Cd but also induced a distinct accumulation of macro- and micronutrients, leading to ion homeostasis (L. Zhang et al., 2023). In this study, we further investigated the potential of the same two MBs, one containing the PGPR *Pseudomonas* sp. strain So_08 and one AMF-based product containing *Rhizoglomus irregulare* BEG72 and *Funneliformis mosseae* BEG234, under combined exposure to Cd and Zn. To this end, the morpho-physiological parameters, oxidative status, untargeted metabolomics of root exudates, ionomics, and metataxonomic analysis were performed.

Overall, this study aims to provide an integrated, multi-omics assessment of PGPR- and AMF- biostimulant-mediated mitigation responses under combined Cd and Zn stress. By linking plant performance, metal partitioning, root exudation patterns, and microbial community dynamics, this work contributes to a mechanistic understanding of microbe-mediated alleviation of HM toxicity in crop systems.

Materials and methods

Biostimulant sources and characteristics

The bacterial biostimulant consisted of a metal-tolerant *Pseudomonas* sp. strain So_08 originally isolated from HMs-impacted soils. The strain was selected among others on the basis of its ability to withstand elevated concentrations of Zn and Cd, as well as the expression of multiple plant growth-promoting traits. These include phosphate solubilization and siderophore production. The bacterial strain was cultivated in sterile conditions using Tryptic Soy Broth (TSB) medium while shaking on an orbital shaker at 180 rpm at 28 °C for 24 h. Following this, sterile water was used to resuspend the pure bacterial biostimulant suspension, which served as the inoculum and was applied to the plants at a final concentration of 10^9 CFU/mL. The fungal biostimulant was a commercial arbuscular mycorrhizal formulation containing *Rhizoglomus irregulare* BEG72 and *Funneliformis mosseae* BEG234, obtained from ATENS Agrotecnologia Naturales SL (Tarragona, Spain), and contains 700 spores g^{-1} of each species. The formulations were applied according to label recommendations, i.e., one application at the dosage of 0.1 g/plant (L. Zhang et al., 2023).

Experimental design

Homogenous and healthy seedlings of tomato (*Solanum lycopersicum* L., cv. Heinz 3402) at the four-true leaves stage were transplanted into pots (15 × 12.5 cm) and grown under field conditions for 52 days. A mixture of soil and sand in a 1:1 ratio, consisting of 65% natural fine peat (Vigorplant Italia Srl, Fombio, LO, Italy), was used. The soil characteristics include a pH of 7.5, electrical conductivity of 0.4 dS m^{-1}, density of 180 kg m^{-3}, and total porosity of 87% v^{-1}. Plants' irrigation was performed every day.

The treatments for this experiment included untreated control, Cd+Zn, Cd+Zn+AMF, and Cd+Zn+PGPR. The experiment was performed in a completely randomized design with four biological replicates for each treatment. Specifically, the microbial biostimulants described in section 2.1, AMF and PGPR, were applied through irrigation during transplantation, as previously described (L. Zhang et al., 2025). The plants were allowed to develop the symbiotic interaction with the AMF and PGPR for two weeks and received a half-strength Hoagland solution. HMs were applied five times (once a week) to gradually reach final concentrations of 100 and 400 mg kg-1 for Cd and

Zn, respectively (both from Merck KGaA, Darmstadt, Germany) (Alengebawy et al., 2021). The selected concentrations were considered to represent an environmentally polluted scenario, representative of a markedly contaminated soil. For Cd, although background concentrations in agricultural soils are generally much lower, values approaching or exceeding 100 mg kg^{-1} have been reported in heavily polluted areas, and this level has also been indicated as a severe contamination threshold for agricultural soils (Voglar and Leštan, 2010). For Zn, while its natural concentration in soils typically ranges between 10 and 300 mg kg^{-1}, concentrations well above 400 mg kg^{-1} have been documented in contaminated environments, particularly in soils affected by mining and smelting activities (Mertens and Smolders, 2013).

The experiment was performed outdoors from 1st June 2021 to 22nd July 2021 at the experimental station of Università Cattolica del Sacro Cuore (Piacenza, Italy). Piacenza is located 51 m above sea level. The average daily thermometric observations for June and July are reported in our previous work (L. Zhang et al., 2023). Given the high evaporative demand during the experimental period, pots were irrigated daily with approximately 500 mL of water per pot to avoid the onset of water deficit and to minimize the influence of irrigation as a confounding factor. The same watering regime was applied to all treatments throughout the experiment. For biomass, the fresh weight (FW) of shoots was measured immediately after sampling, while root samples were weighed after washing with tap water and drying. Dry weight (DW) was determined after 48 h at 65 °C. Further analyses were conducted as outlined in the following sections.

Physiological parameters

Three physiological parameters, including relative water content (RWC), leaf membrane stability index (MSI), and photosynthetic performance, were measured. For RWC, a fully expanded leaf from each of the four replicates was collected and weighed as fresh weight (FW), and then floated in 15 mL ultrapure water for 24 h at 4 °C for full hydration (TW). The leaves were then oven-dried (at 70 °C for 2 days) and weighed as dry weight (DW). RWC was then calculated following the equation: = (FW-DW)/(TW-DW) × 100.

The membrane stability index (MSI) was determined following the method described by Sairam et al. (2002). Two healthy leaves from each of the four plants were individually placed in test tubes containing 5 mL of ultrapure water and heated for 30 min at 30 °C. The electrical conductivity was read as EC1. Subsequently, the samples were heated for an additional 30 min at 100 °C, cooled on ice, and the electrical conductivity was recorded as EC2. The MSI index was calculated using the following equation: MSI (%) = (EC1/EC2) × 100.

Fluorescence activity and chlorophyll content assessments were conducted at three specific time points: on the 16th day, 23rd day, and 30th day after the treatment (DAT). The measurements of three parameters, including *Fv/Fm* (maximum quantum yield of PSII), *PI abs* (performance index), and SPAD (Chlorophyll content), were made on fully expanded leaves following a dark adaptation performed using clips. Pocket PEA Chlorophyll Fluorimeter instrument (Hansatech Instruments Ltd, King's Lynn, UK) and Chlorophyll Meter SPAD- 502Plus (Konika Minolta) were used for fluorescence activity and chlorophyll measurements, respectively.

Root phenotyping

At the end of the trial, the roots were thoroughly cleaned with tap water and stored in plastic containers filled with distilled water at 4 °C in the fridge until the measurements were taken. The TWAIN interface at 600 dpi was used with a scanner (Epson Expression 10000xl) equipped with a double light source for scanning the roots. The analysis of root morphology was performed using winRHIZO Pro software (2019), considering parameters such as root diameters (mm), Root Length Density (RLD; cm/cm^3), Specific Root Length (SRL; m/g), Root Surface Volume Density (RSVD; mm^3/cm^3), Specific Root Area Density (SAD; cm^2/cm^3), Specific Root Surface Area (SSA; cm^2/g), Root Volume Density (RVD; cm^3/cm^3), and Root Tissue Density (RTD; g/cm^3).

Root arbuscular mycorrhiza fungi colonization

For each experimental group, four replicates were analyzed to quantify AMF colonization in the tomato roots. Samples were first washed, and subsamples were then collected for the assessment of mycorrhizal colonization. The roots were cleared in 10% (w/v) KOH and stained with 0.05% (w/v) trypan blue prepared in lactophenol. Subsequently, AMF colonization was examined under a stereomicroscope (Leica EZ4V, 32 ×; Leica Microsystems Srl, Buccinasco, Italy). The proportion of colonized root segments was estimated using the gridline intersect method (Bonini et al., 2020).

In-situ detection of H_2O_2 and O_2^-

The in-situ accumulation of hydrogen peroxide (H_2O_2) and superoxide anion (O_2^-) in leaves was assessed histochemically using 3,3′-diaminobenzidine (DAB) and nitro blue tetrazolium (NBT) staining, respectively, following previously described methods with minor modifications (Araniti et al., 2020; Martos et al., 2025). Fully expanded leaves were detached from each plant and briefly rinsed with distilled water. For H_2O_2 detection, leaves were incubated in the dark in a DAB solution (1 mg mL^{-1}, pH 3.8) for 8 h. After incubation, the leaves were exposed to light for 30 min to enhance stain development. For O_2^- detection, leaves were incubated in an NBT solution (2 mg mL^{-1} in 50 mM sodium phosphate buffer, pH 7.5) in the dark overnight at room temperature. After staining, chlorophyll was removed by immersing the leaves in ethanol:acetic acid (1:1, v/v) until complete decolorization. The stained tissues were then photographed against a contrasting background. H_2O_2 accumulation was visualized as a reddish-brown precipitate, whereas O_2^- accumulation was detected as a dark blue formazan deposit.

High-throughput sequencing and metataxonomic analysis

The rhizosphere soil was collected by gently shaking the roots to remove bulk soil and retaining the soil that tightly adhered to the root surface. Total DNA was extracted from 500 mg of rhizosphere soil using the FastDNA™ SPIN Kit for Soil (MP Biomedicals, Santa Ana, CA, USA), following the manufacturer's instructions. DNA concentration was quantified using a Qubit™ fluorometer with the Quant-iT™ HS dsDNA assay kit (Invitrogen, Waltham, MA, USA).

Bacterial communities were profiled targeting the V3-V4 region of the 16S rRNA gene, while fungal communities were characterized by amplifying the ITS1 region. Amplicons were generated using barcoded universal primers for bacteria and fungi, respectively, following a nested PCR strategy as reported in the supplementary material. PCR products were pooled, purified using a solid-phase reversible immobilization (SPRI) method. Library preparation was carried out by Fasteris S.A. (Geneva Switzerland) using the TruSeq DNA Sample Preparation Kit (Illumina Inc., San Diego, CA, USA) for amplicon library preparation, and sequenced with MiSeq Illumina instrument (Illumina Inc., San Diego, CA), generating 300 bp paired-end reads. The fastq reads processing, QC, and demultiplexing are described in the supplementary material. Taxonomic assignments were conducted using a naïve Bayes classifier within the QIIME 2 feature-classifier plugin (Estaki et al., 2020). Bacterial ASVs were classified against the SILVA v119 database, trained on the V3-V4 region, while fungal ASVs were assigned taxonomy using the UNITE v8 database. The resulting ASV tables and taxonomic annotations were used for downstream diversity and community composition analyses using MicrobiomeAnalyst v3.0 (https://www.microbiomeanalyst.ca) as the primary platform (Chong et al., 2020). ASVs abundance tables generated in QIIME2 were

imported, and low-abundance features were filtered to reduce noise and sequencing artifacts. Data were subsequently rarefied to a common sequencing depth to account for uneven sequencing depth among samples.

Predictive functional profiling of the bacterial community was performed using PICRUSt2 v2.5.1, available at https://github.com/picrust/picrust2 (Douglas et al., 2020). The analysis was carried out on the 16S rRNA gene amplicon dataset after sequence processing and reads quality check. Briefly, PICRUSt2 was used to infer the putative functional potential of the bacterial communities from ASV abundance data by placing representative sequences into a reference phylogeny and predicting pathway abundances for each sample. Predicted functional profiles were subsequently explored at the level of metabolic pathways. Functional annotations were assigned using the MetaCyc pathway databases (Caspi et al., 2016). Downstream comparison and visualization of predicted functional profiles were performed using STAMP v2.3.1. Since this approach is based on functional inference from marker-gene data, the results were interpreted as putative functional potential rather than direct metagenomic evidence.

Ionomics analysis

The plant tissues were dried at 65 °C until constant weight and, afterward, mineralized with 69% ultrapure HNO_3 (Carlo Erba, Milano, Italy) in a single-reaction-chamber microwave digestion system (UltraWAVE, Milestone, Shelton, CT, USA). The digested samples were diluted with ultrapure water (18.2 MΩ·cm) until 2% HNO_3, and then, concentrations of macro and micronutrients were determined using an inductively coupled plasma–mass spectrometer (ICP-MS, iCAP™ _RQ, Thermo Scientific). Element quantification was carried out using certified multi-element standards (CPI International, https://cpiinternational.com). Accuracy and matrix effect errors were checked using NIST standard reference material 1573a (tomato leaves) and 1570a (spinach leaves), which were digested and analyzed applying the same protocol as for samples of plant tissues. The analyses were carried out on three independent biological replicates. To evaluate the internal redistribution of heavy metals, translocation factors (TF) were calculated as follows: $TF = C_{shoot} / C_{root}$, where C_{shoot} represents the metal concentration in the above-ground tissues (leaves or fruits) and C_{root} represents the metal concentration in roots. TF values were calculated separately for root-to-leaf and root-to-fruit translocation for both Cd and Zn. Bioconcentration factor (BCF) was calculated as $BCF = C_{plant} / C_{soil}$, where C_{plant} represents the metal concentration in plant tissues (root, leaf, or fruit) and C_{soil} represents the corresponding metal concentration in soil. Given the combined Cd+Zn treatment, BCF values were calculated separately for each element using their respective soil concentrations (Cd = 100 mg kg^{-1}; Zn = 400 mg kg^{-1}). BCF was calculated only for contaminated treatments, as control soils did not receive Cd or Zn addition and would result in undefined values.

Root exudates analysis

After removing the plants from the pots, the roots were carefully washed with tap water to remove any soil particles and debris and then transferred to plastic containers filled with distilled water. Root exudates were collected for 4 h continuously, with the solution aerated, and the pots were covered with aluminum foil to keep the roots in the dark. This methodology was previously optimized and reported in several works (L. Zhang et al., 2025). After 4 h, the root exudate solutions were centrifuged at 5000 *x g* for 15 min, filtered through a 0.22 μm filter, and freeze-dried for the following analysis. 50 mL of freeze-dried exudate solution was re-suspended in 1 mL of 50% methanol (v/v), and the exudate profiling was conducted using a 6560-drift tube-ion mobility-quadrupole-time of flight-high resolution mass spectrometer (DTIM-UHPLC-QTOF-HRMS; Agilent Technologies, Santa Clara, CA, USA) with an injection volume of 19 μL, as described in detail in the Supplementary Materials. Data annotation and MS/MS structural confirmations were performed with MS-DIAL software (version 4.90). This process involved automated peak detection (against pooled QC) and putative annotation through spectral matching with accessible databases such as BMDMS-NP and the Fiehn/Vaniya natural product library, as detailed in the supplementary materials. According to the Metabolomics Standards Initiative (MSI), these annotations correspond to confidence Level 2, i.e. putatively annotated compounds, and not to confirmed identifications based on authentic standards (Salek et al., 2013).

Statistical analysis

Univariate statistical analyses of morpho-physiological parameters and vegetative indices were performed in IBM SPSS, with Tukey's post hoc test applied ($p < 0.05$) to identify significant differences among different treatments. The correlation between the overall ionic profile and plant morpho-physiological parameters using rCCA (regularized Canonical Correlation Analysis) with the mixOmics package in R (version 4.2.2), as well as Spearman correlation between ionic profile using "corrplot". The same R package was used to integrate multi-omics data (root exudate profile and soil microbial population profile) following the DIABLO (Data Integration Analysis for Biomarker Discovery using Latent Variable Approaches for Omics Studies) framework, using parameters previously optimized (L. Zhang et al., 2025). Specifically, the number of components resulting from the tuning process for the sPLS-DA (sparse Partial Least Squares Discriminant Analysis) model was two components using the Mahalanobis distance, considering 12 and 24 features for the metabolomics dataset, 15 and 10 for the bacterial dataset, and 10 and 15 for the fungal dataset, as the first and second components, respectively.

Metabolomics data were processed with Mass Profiler Professional 12.6 (Agilent Technologies). Raw values were log2-transformed, normalized to the 75th percentile, and median-centered per compound. Treatment-specific patterns were explored through both unsupervised and supervised multivariate approaches: hierarchical cluster analysis (HCA) was applied to reveal grouping trends, while orthogonal projections to latent structures discriminant analysis (OPLS-DA) was used to identify discriminant markers. Variables with VIP scores > 1.2 were retained as significant markers in each pairwise comparison against the control. These markers were further refined using a Venn diagram, and the differentially expressed metabolites were classified by their chemical structure.

For α-diversity, differences between samples were assessed using the Chao1 richness index. Statistical differences among treatments were evaluated by one-way analysis of variance (ANOVA) in MicrobiomeAnalyst v3.0. Pairwise comparisons were carried out in R (version 4.4.2) using the RStudio environment with Tukey's Honestly Significant Difference (HSD) test. β-diversity was evaluated using Bray–Curtis dissimilarity, with group differences tested by pairwise PERMANOVA, and community-level differences were visualized by principal coordinates analysis (PCoA). Differential abundance of microbial taxa across treatments was evaluated using the Linear Discriminant Analysis Effect Size (LEfSe) algorithm. LEfSe was performed with default settings at the genus level to identify bacterial and fungal genera that were significantly impacted by HMs or MBs applications based on both statistical significance and effect size.

Results

Changes in biomass and root morphology in response to HMs exposure, biostimulants, and AMF colonization

The effect of Cd+Zn pollution on tomato morphological parameters was determined by assessing both shoot and root biomass (Fig. 1A), considering fresh weight (FW) and dry weight (DW) (Fig. 1B, C), as well

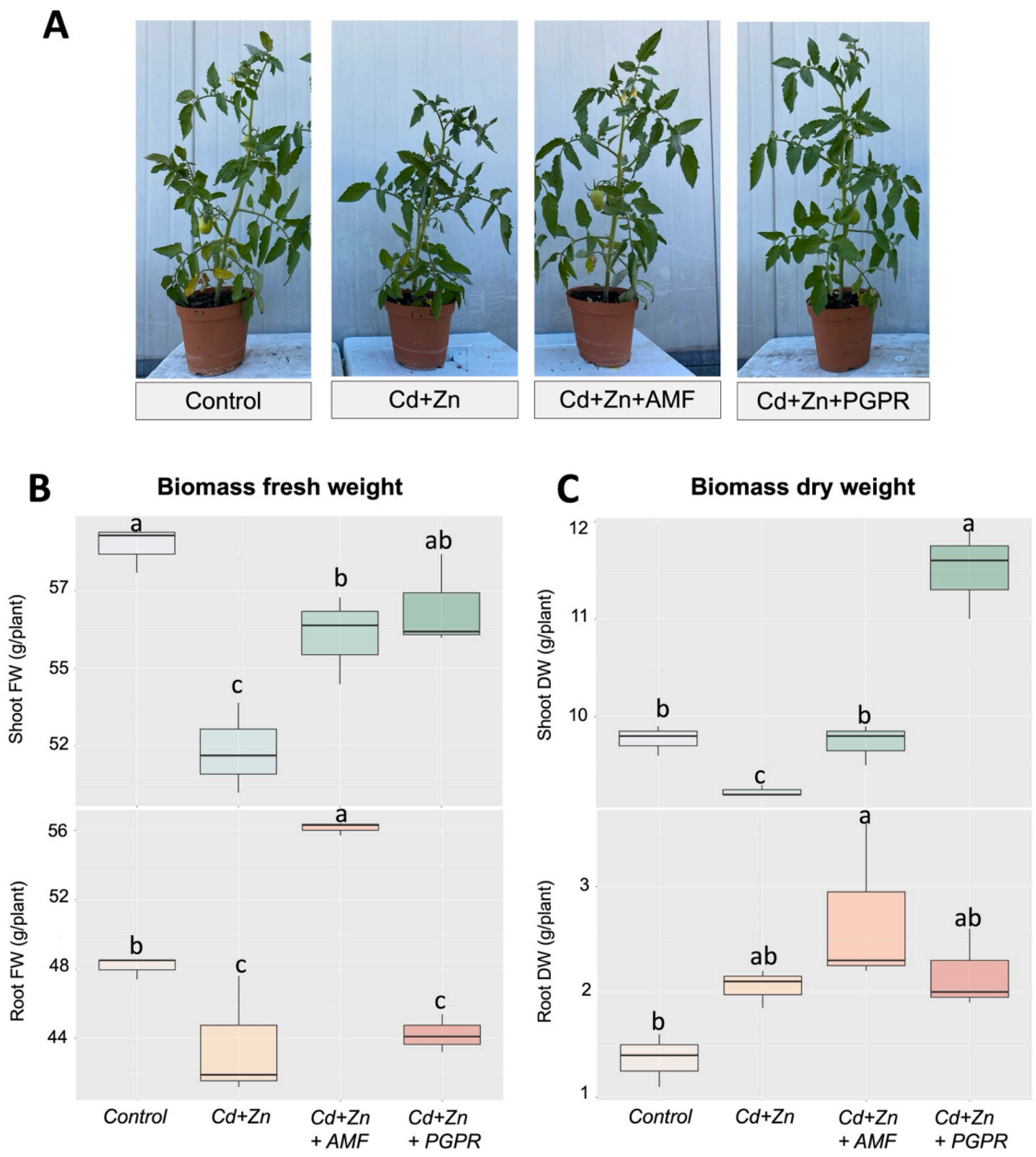

Fig. 1. Images of tomato plants under control, Cd+Zn, Cd+Zn+AMF, and Cd+Zn+PGPR treatments at the end of the experimental period (52 days after transplant) (A), along with the average fresh (B) and dry (C) weights of shoot and root tissues.

as root morphology and architecture (Figure. S1). Furthermore, AMF root colonization was assessed (Figure. S2) and confirmed, with an average of 25%.

The results indicated a significant impact of treatments on biomass, with the Cd+Zn treatment leading to a notable decline in both FW and DW of shoots, while only FW of roots declined (Fig. 1B, C). However, the application of AMF and PGPR positively affected biomass recovery. Notably, PGPR treatment mainly increased shoot FW and DW, while AMF treatment increased root tissues.

Root morphology analysis showed that two parameters, RLD and SAD, among others, were statistically significant, with the Cd+Zn treatment increasing them (Figure. S1c, f), which were restored by the application of AMF and PGPR, suggesting modulation of root growth in response to induced toxicity. The other root-related parameters did not show statistically significant differences.

The effect of treatments on physiologically related parameters

The physiological response of tomato to Cd+Zn stress was evaluated using RWC (Fig. 2A), MSI (Fig. 2B), *in situ* quantification of H_2O_2 and O_2^- (Fig. 2C), and photosynthetic performance (Fig. 2D).

Cd+Zn stress increased RWC, whereas the Cd+Zn+PGPR treatment had the lowest value compared to the control (Fig. 2A). In contrast, Cd+Zn reduced MSI compared to the control, while AMF and PGPR mitigated this reduction by increasing MSI (Fig. 2B).

The in-situ assays for H_2O_2 and O_2^- showed increased accumulation of ROS species in Cd+Zn-treated leaves, as indicated by stronger color development, particularly in the lower leaf regions. In contrast, PGPR application reduced the accumulation of these H_2O_2 species, as reflected by the weaker color intensity. The AMF enabled the reduction of O_2^- species accumulation relative to H_2O_2 (Fig. 2C).

Fv/Fm, PI*abs*, and SPAD, key indicators of photosynthetic performance, were measured (Fig. 2D). Significant changes in these

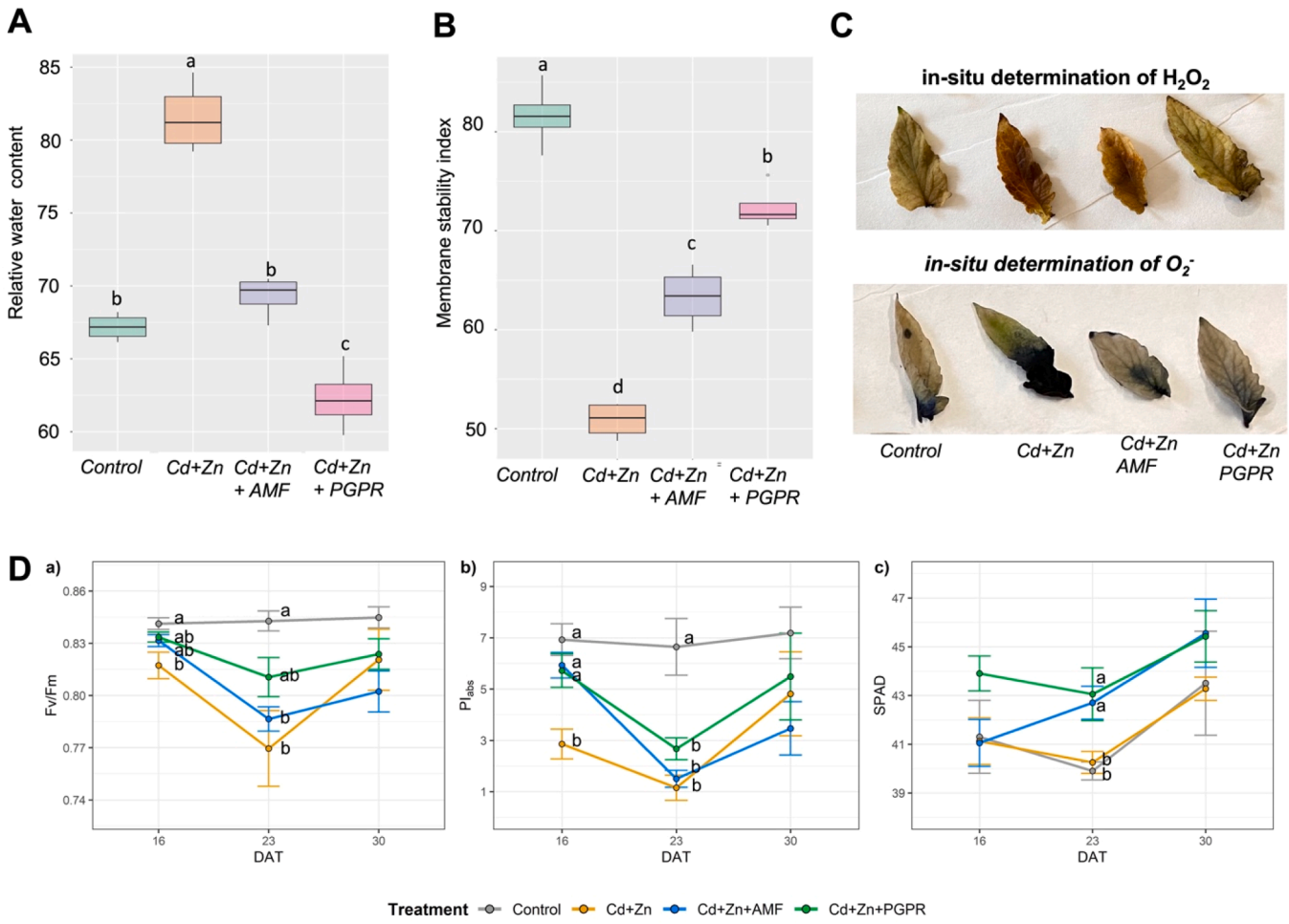

Fig. 2. Physiological parameters, including relative water content (A), membrane stability index (B), images of *in situ* determination of H2O2 and O2- (C), and photosynthetic parameters such as Fv/Fm, PIabs, and SPAD (D).

parameters were observed at 16, 23, and 30 DAT. Cd+Zn consistently reduced *Fv/Fm* and PI*abs* at all measurement points, indicating an inhibitory effect on photosynthesis. In contrast, the application of MBs, especially PGPR, slightly improved these parameters compared to the Cd+Zn treatment. By 30 DAT, both *Fv/Fm* and PI*abs* increased in the Cd+Zn treatment and in its combination with MBs, suggesting the development of a tolerance mechanism over time. Regarding the SPAD index, a significant difference was observed only at 23 DAT, with a general increase in SPAD values in plants treated with HMs in combination with MBs.

Ionomic profiling of tomato organs under varied treatments

An assessment of the comprehensive ionomic composition in the roots, leaves, and fruits of tomato plants was performed to ascertain the impact of MBs on the absorption and distribution of mineral nutrients. Exposure to Cd+Zn significantly affected the accumulation of Cd and Zn in all tomato organs (Fig. 3A). Generally, the trend of Cd accumulation in the Cd+Zn treatments follows the sequence: root > leaf > fruit. Interestingly, the application of MBs markedly mitigated Cd content, particularly significant in roots and fruits. Comparing the two MBs, the results showed that PGPR mitigated Cd accumulation in roots and leaves more effectively (Fig. 3A). In contrast, Zn allocation decreased in roots and leaves after MBs application, while a contrasting effect was observed in fruits.

In the context of macronutrient composition, there was evident tissue-specific accumulation. For instance, the relative content of Ca exhibited a significant increase following Cd+Zn treatment in all tomato tissues (Fig. 3C, Supplementary Table S1). Conversely, its concentration decreases slightly with the application of MBs, although it remains higher than in the control group. Magnesium (Mg) showed a similar trend in fruits. As for sodium (Na), its relative abundance increased in all tissues except for roots, particularly in Cd+Zn treatment. A general decline in phosphorus (P) and potassium (K) content was observed in fruits, contrasting with an increased P in roots across all treatments compared to the control group. Remarkably, AMF application led to a significant decrease in P content in fruits.

Regarding the micronutrient concentration in plants following exposure to HMs and MBs, increased concentrations of iron (Fe) and nickel (Ni) were observed in roots when HMs were combined with AMF, whilst the inoculation with PGPR induced accumulation levels comparable to the control (Fig. 3D, Supplementary Table S1). The content of copper (Cu) and manganese (Mn) in the roots of HMs-exposed plants was also reduced when the MBs were applied. Additionally, the use of both MBs significantly decreased the content of Fe, Mn, Mo, and Cu in the leaves of tomato plants exposed to HMs. At the fruit level, the inoculation with AMF significantly reduced the content of Ni, whilst the PGPR reduced the allocation of Cu (Supplementary Table S1).

To assess this redistribution, translocation factors (TF) from roots to leaves and fruits were calculated (Table 1). Under control conditions, Cd and Zn exhibited relatively high mobility towards leaves (TF > 1), while Cd translocation to fruits remained limited. Exposure to Cd+Zn drastically reduced metal mobility, with Cd TF to leaves decreasing by approximately 88% and to fruits by 66% compared to the control. A

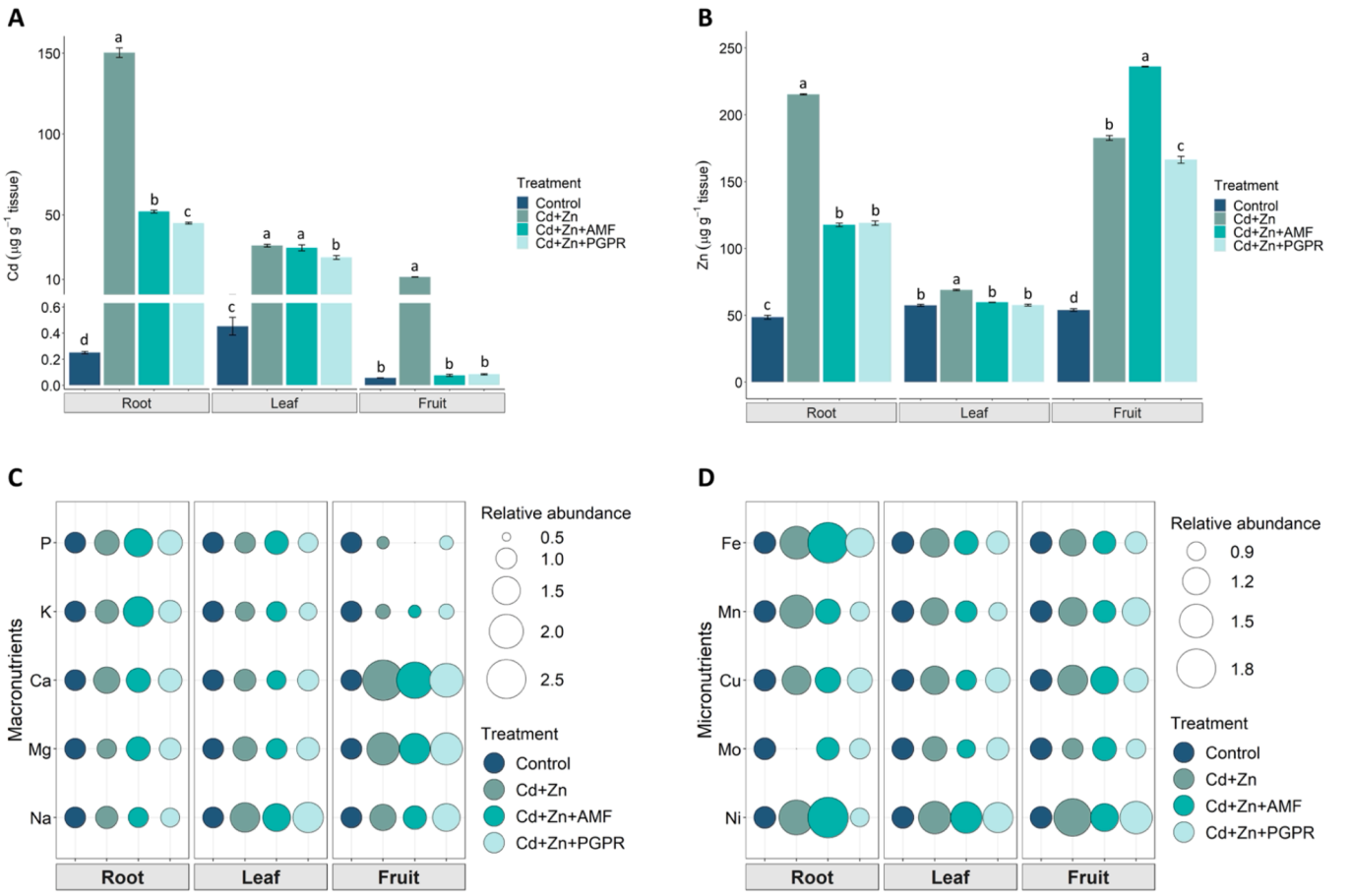

Fig. 3. Ionomic profile of root, leaf, and fruit tissues of tomato plants. (A) The concentration of Cd and (B) Zn in tomato plants grown under combined exposure of Cd and Zn, either non-inoculated or inoculated with AMF or PGPR. (C) Relative abundance of macronutrients and (D) micronutrients in tomato plants grown under combined Cd+Zn stress, either non-inoculated or inoculated with AMF or PGPR. Relative abundance was calculated by normalizing the concentration of each nutrient across all treatments to that in the non-inoculated control treatment. Differences between means were determined by Tukey's HSD test. Different letters indicate statistically different values ($p < 0.05$). The concentration data are reported in Supplementary Table S1.

Table 1
Translocation factor (TF) of Cd and Zn from roots to leaves and fruits in tomato plants under different treatments.

Treatment	Cd TF		Zn TF	
	root-to-leaf	Root-to-fruit	root-to-leaf	Root-to-fruit
Control	1.788 ± 0.206 a	0.227 ± 0.001 a	1.185 ± 0.030 a	1.112 ± 0.034 c
Cd+Zn	0.206 ± 0.005 b	0.077 ± 0.000 b	0.320 ± 0.002 c	0.848 ± 0.009 d
Cd+Zn+AMF	0.571 ± 0.045 b	0.001 ± 0.000 c	0.507 ± 0.004 b	2.006 ± 0.023 a
Cd+Zn+PGPR	0.527 ± 0.019 b	0.002 ± 0.005 c	0.485 ± 0.011 b	1.398 ± 0.004 b

TF was calculated as the ratio between metal concentration in above-ground tissues (leaf or fruit) and roots. Values are expressed as mean ± standard error (SE). Different lowercase letters indicate significant differences among treatments within each column (Tukey's HSD test, $p \leq 0.05$).

similar trend was observed for Zn, with reductions of about 73% (root to leaf) and 24% (root to fruit). The application of microbial biostimulants (MBs) significantly modified these patterns (Table 1). Both AMF and PGPR partially restored Cd translocation to leaves compared to Cd+Zn alone (increases of approximately 2.8-fold and 2.6-fold, respectively), although values remained about 3-fold lower than the control. In contrast, Cd translocation to fruits was almost completely suppressed by MBs, showing reductions of >99% relative to control. For Zn, TF from root to leaf increased under MB treatments compared to Cd+Zn alone (+8% with AMF and +2% with PGPR), although values remained approximately 57–59% lower than those observed in the control. Notably, Zn allocation to fruits exhibited a contrasting response. AMF induced a strong increase, with TF values approximately 80% higher than the control and 137% higher than Cd+Zn, while PGPR also enhanced Zn translocation to fruits, reaching 26% above the control and 65% above Cd+Zn (Table 1). Consistently, bioconcentration factor (BCF) analysis indicated that Cd accumulation was mainly confined to roots (BCF > 1 under Cd+Zn), while its accumulation in fruits was strongly reduced by MBs, whereas Zn showed moderate accumulation with enhanced allocation to fruits, particularly under AMF treatment (Supplementary Table S2).

To further explore the relationships among mineral elements, a Spearman correlation analysis was performed and is reported in Supplementary Figure. S3. Significant positive correlations were detected among several metals, including Cd with Fe, Zn, and Ni, and Zn with Ni, suggesting a coordinated accumulation pattern under the experimental conditions. Additional positive correlations were observed among Mg, Mo, Ca, and Cu, whereas K was negatively correlated with Zn, Na, and Cu. In contrast, no significant correlation was found between Ca or P and Cd/Zn, indicating that the increased accumulation of Ca and P observed in roots under metal stress cannot be directly interpreted, in this dataset, as evidence of a specific Ca/P-mediated alleviation mechanism.

rCCA correlation analysis between physiological and ionomic parameters

Regularized canonical correlation analysis (rCCA) was performed to identify the relationships between physiological parameters and the ion profile (Fig. 4). The score plot showed a clear separation between the control group and the treatments, particularly Cd+Zn and its combination with AMF, while Cd+Zn+PGPR was closer to the control (Fig. 4A). The network analysis further revealed that Cd was negatively correlated with MSI, while positively correlated with sodium accumulation and root parameters like RSVD, RLD, and RVD (Fig. 4B). Similarly, Ni exhibited a negative correlation with MSI and positive correlations with RSVD, SAD, RLD, and RVD. Regarding Fe, the negative correlation with MSI was highlighted.

Root exudate metabolic profiling using UHPLC-QTOF/MS

Root exudates were profiled using UHPLC-QTOF/MS, resulting in the annotation of 1164 compounds, showing notable chemical diversity (Table S3). These compounds belonged to different metabolite classes, including amino acids, lipids, sugars, organic acids, phenolic compounds, N- and S-containing compounds, and alkaloids. Afterward, the unsupervised hierarchical cluster analysis (HCA) and Partial Least Squares Discriminant Analysis (PLS-DA) models were used to assess overall differences among the sample treatments, revealing a clear separation among the four groups (Figure. S4). Specifically, the treatment with Cd+Zn+PGPR accounted for the most discriminant variance, while the application of AMF resulted in a more closed exudate profile than the HM-stressed one. Finally, OPLS-DA modeling was performed to identify the most discriminant markers associated with single treatments, using pairwise comparisons between Cd+Zn, Cd+Zn+AMF, and Cd+Zn+PGPR relative to control (Fig. 5). The model revealed a clear separation between treatments and the control, as reflected by high values of the goodness-of-fit (R^2Y) and predictive ability (Q^2Y) parameters. The metabolites with variable importance in projection (VIP) scores > 1.2 that passed the one-way analysis of variance (ANOVA) threshold ($p < 0.05$) were then used in the Venn analysis to identify the unique VIP markers for each treatment. These metabolites were then integrated with logFC values (Table S4) and assigned to metabolite classes to interpret the modulation trends in the treatments.

As shown in Fig. 5B, the discriminant metabolites belonging to various classes were differentially modulated by the treatments. The combination of Cd+Zn with MBs, particularly PGPR, resulted in a higher number of discriminant and modulated metabolites. The Cd+Zn treatment alone caused a general decrease in the accumulation of amino acids, N-containing compounds, alkaloids, and isoprenoids. Among VIP markers in Cd+Zn, some metabolites related to secondary metabolism, such as chlorogenic acid (LogFC = 2.9), Xanthohumol (LogFC = 4.2), di-*O*-methylfraxetin, heptadecanoic acid, and dehydroabietic acid were accumulated, while syringic acid and spermidine were down-accumulated. Conversely, the pathway analysis revealed a general accumulation of almost all metabolite classes in Cd+Zn+AMF, whereas both up- and down-modulation were observed in the treatment combined with PGPR. Notably, lipid metabolites (such as ricinoleic acid, stearic acid, and pentacosanoic acid) and phenylpropanoids were down-modulated. In contrast, steroidal saponins (such as Polyphyllin VI), lignans (such as 7,8-dihydromethysticin), and N-containing compounds (such as Dehydroevodiamine and Wulignan A1) were accumulated. Regarding the Cd+Zn+AMF treatment, cofactors such as pyridoxine (LogFC = 1.2) and biotin (LogFC = −1.5), Tanshinone IIA (a diterpenoid), and sinapine (a phenolic) were among the significant VIP markers.

Effects of HM stress and MBs on rhizosphere microbial diversity and taxonomic composition

Amplicon sequencing of bacterial communities yielded a total of 304,036 high-quality reads, with an average of 25,336 reads per sample. The sequencing depth ranged from 14,340 to 41,526 reads per sample. To account for differences in sequencing depth among samples, data were rarefied to a library size of 13,765 reads, which retained all samples for downstream analysis.

Alpha-diversity analysis revealed significant differences in bacterial richness among treatments. The highest bacterial diversity was observed in rhizosphere samples treated with the PGPR *Pseudomonas* So_08, which showed significantly higher Chao1 values compared with the control ($p < 0.01$) and a non-significant trend toward higher richness relative to the other treatments (Fig. 6). In contrast, the AMF application resulted in bacterial diversity values comparable to those of the control, which exhibited the lowest overall richness. Interestingly, exposure to combined HMs increased bacterial α-diversity relative to control conditions, although this increase did not reach statistical significance.

In contrast to α-diversity, β-diversity analysis based on Bray–Curtis dissimilarity did not reveal significant differences among treatments. PCoA showed substantial overlap among samples, indicating a broadly similar bacterial community composition across treatments (data not shown). Despite this overall compositional stability, LEfSe analysis identified 41 bacterial genera that were differentially abundant among treatments, revealing treatment-specific taxonomic shifts (Fig. 6). The genus *Geobacillus* was significantly enriched under combined HM exposure, while exhibiting the lowest relative abundance in control samples. *Bacillus* were most abundant in AMF-treated samples, suggesting a potential synergistic association between AMF colonization

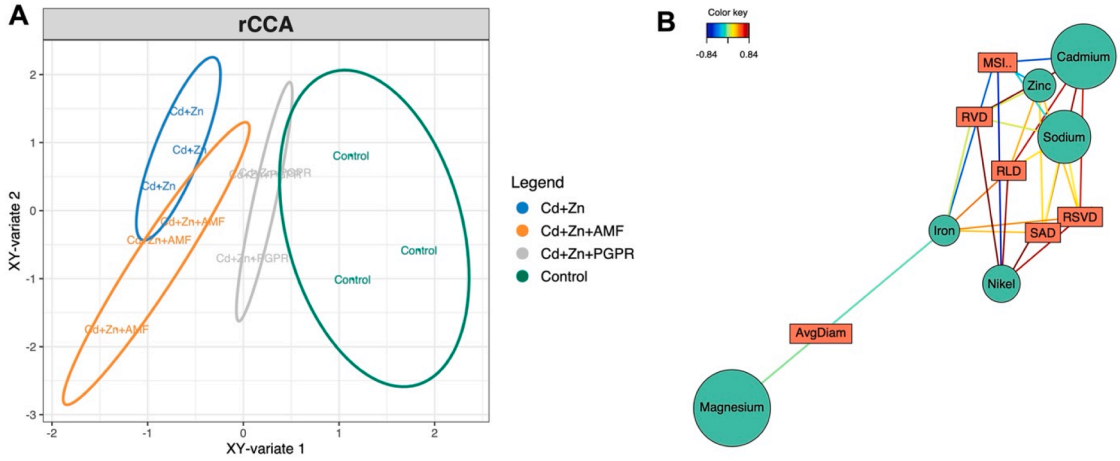

Fig. 4. Regularized canonical correlation analysis (rCCA) score plot (A) and correlation network (B) of the most correlated features (|r = 0.85|).

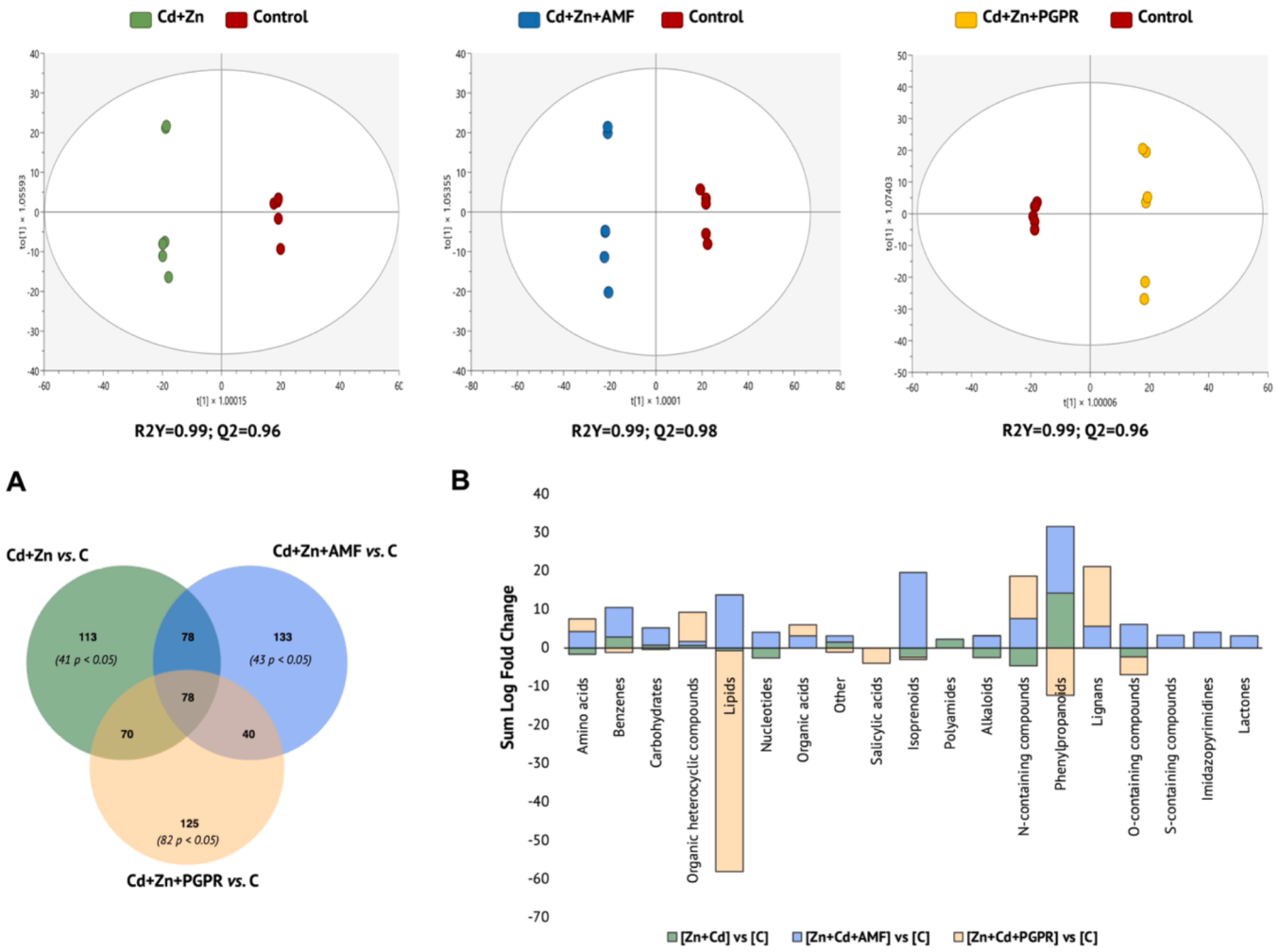

Fig. 5. Score plots of the OPLS-DA model on the untargeted metabolomics profile of root exudates, showing pairwise comparisons between the treatments and the control group. Venn diagram of VIP markers derived from the OPLS-DA models (A), and their classification based on compound ontology (B). Abbreviation: AMF = Arbuscular Mycorrhizae Fungi, PGPR = Plant Growth Promoting Rhizobacteria, C = Control.

and spore-forming, stress-resilient bacteria. In contrast, *Rhabdanaerobium* and *Dokdonella* were predominantly enriched in rhizosphere samples inoculated with the PGPR strain So_08, suggesting a potential contribution of these taxa to nutrient cycling and detoxification processes under Cd+Zn exposure. In addition, members of the genus *Flavobacterium* were abundant in control rhizospheres and were depleted in the presence of HMs. In particular, their abundance increased after PGPR inoculation and, even more markedly, with the addition of AMF despite combined HM stress, indicating a partial recovery of this taxon.

At the fungal level, α-diversity patterns mirrored those observed for bacteria, with PGPR-treated samples showing higher Chao1 richness than the control ($p < 0.05$), while AMF and HM treatments showed intermediate values (Fig. 6). Furthermore, different α-diversity indices, including ACE, Shannon, and Simpson, are presented in supplementary Table S5. LEfSe analysis further revealed distinct fungal taxa associated with each treatment, including enrichment of *Rozellomycota* and *Mortierellaceae* in Cd+Zn- and Cd+Zn+AMF-treated samples, taxa commonly linked to organic matter turnover and stress-adapted saprotrophic lifestyles. While *Eurotiales* and *Corynascella* were more associated with the application of PGPR and AMF. Collectively, these results indicate that while overall community structure remained relatively stable, both PGPR and AMF application selectively reshaped the rhizosphere microbiome by promoting specific bacterial and fungal taxa potentially involved in nutrient cycling, organic matter degradation, and heavy-metal stress mitigation.

Although β-diversity analysis did not indicate a significant separation of the overall bacterial community structure among treatments, differential abundance analysis revealed selective changes in specific bacterial and fungal taxa. This suggests that Cd+Zn stress and MBs application did not induce a broad restructuring of the rhizosphere microbiome, but rather affected defined microbial groups within an overall stable community background.

PICRUSt2-based functional prediction revealed significant treatment-dependent differences in the putative functional potential of the bacterial rhizosphere community (Figure. S5). Among the predicted pathways showing significant variation, several were related to aromatic compound transformation. In particular, catechol degradation, aerobic toluene degradation, and the cleavage pathway of aromatic compounds were more represented in the Cd+Zn+AMF treatment than in Cd+Zn alone ($p < 0.05$), indicating that AMF application was associated with a higher predicted bacterial potential for aromatic compound turnover under combined metal stress. In the Cd+Zn+PGPR treatment, a significant increase was mainly observed for aerobic toluene degradation ($p < 0.05$), whereas the other aromatic-compound-related pathways showed less pronounced differences. In addition, starch degradation was significantly increased in both microbial biostimulant treatments compared with Cd+Zn alone, with the highest predicted values observed under PGPR application ($p < 0.001$). Overall, these results suggest that AMF and PGPR affected the predicted functional potential of the bacterial community, particularly pathways

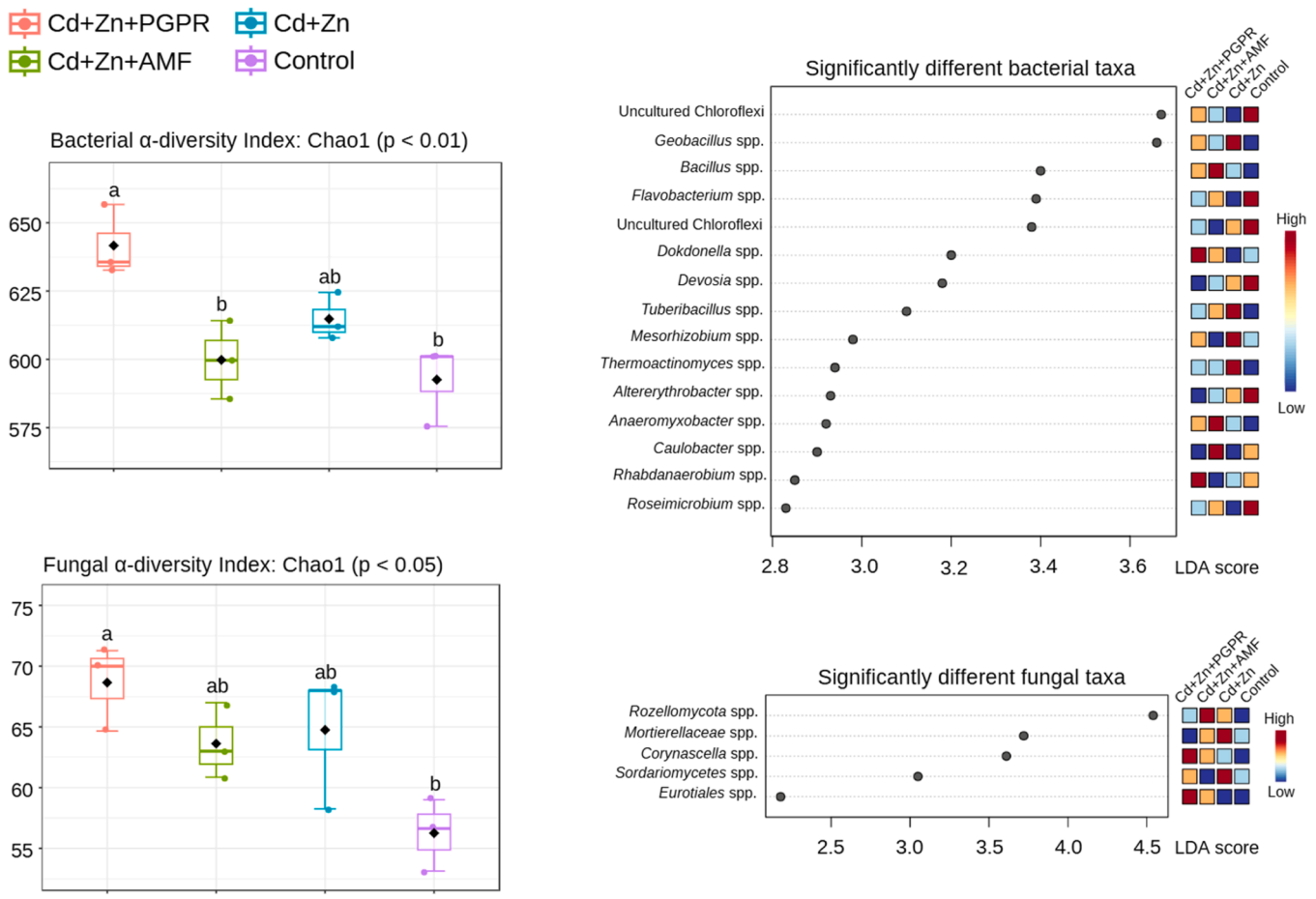

Fig. 6. α-diversity expressed as Chao1 richness index, of bacterial (top left) and fungal (bottom left) communities across treatments, ordered as Cd+Zn+PGPR, Cd+Zn+AMF, Cd+Zn, and Control. Different letters indicate significant differences among treatments. Differentially abundant bacterial (top right) and fungal (bottom right) genera identified by LEfSe analysis are shown with their corresponding linear discriminant analysis (LDA) scores. olored boxes indicate relative enrichment across treatments. Only the main bacterial taxa meeting both statistical significance and effect-size thresholds are displayed.

involved in aromatic compound processing and carbon substrate degradation.

Metabolomics and metagenomics data integration using DIABLO-based model

The DIABLO multi-omics data integration analysis, based on supervised sparse PLS-DA, has been applied to assess the relationships among the three principal variables examined in this study, root exudate profiles and soil fungal and bacterial microbiomes, which revealed strong cross-dataset correlations captured by the two sparse components (Fig. 7c). The most strongly correlated features identified by the analysis are listed in the Supplementary Materials (Table S6), while the top eight features contributing to component 1 are presented in Fig. 7b Interestingly, these features displayed high correlation coefficients among the integrated omics datasets ($r > |0.9|$), for both positive and negative correlations, as visualized in the heat map (Fig. 7a) and network analysis (Fig. 7d).

The omics-integration results highlighted that the application of PGPR to tomato growth under Cd+Zn pollution led to an enrichment of the fungal families Aspergillaceae (ITS23) and Chaetomiaceae (ITS84). These fungi were positively correlated with several exudate metabolites, including sugars (M108), amino acids (M20 and M10), phenolic compounds (M1002, M1029, and M937), terpenoids (M715 and M483), and lipids (M199). The same effect has been observed for bacterial families, where PGPR treatment under Cd+Zn stress induced the accumulation of Flavobacteriales (BAC894) and Polyangiales (BAC857) bacterial orders (Fig. 7d).

On the other hand, the application of AMF to tomato growth under Cd+Zn pollution led to the accumulation of Defluviitaleaceae (BAC759) bacteria (Fig. 7b).

Discussion

Morphophysiological responses of tomato plants to combined Cd and Zn stress

Morphological and physiological parameters are widely recognized as good indicators for estimating plant tolerance to HMs, with growth inhibition among the earliest visible symptoms of metal toxicity (Guo et al., 2020; Noor et al., 2022). In this study, the significant reduction in shoot and root biomass under Cd+Zn treatment clearly indicated that tomato plants were negatively affected by exposure to HMs. Although not statistically significant, most root-related parameters increased under Cd+Zn treatment, possibly reflecting a compensatory adjustment of the root system to provide water and nutrients while regulating the uptake of undesirable substances. Such changes are consistent with known root responses to metal stress, including primary root length and diameter, lateral root density, and lateral root elongation (van Dijk et al., 2022). However, increases in root traits, such as RLD, SRL, SAD, and RVD, were insufficient to prevent biomass decline, suggesting that metal toxicity and reduced nutrient availability ultimately constrained plant growth (Farooq et al., 2022). To further support the negative effect of Cd+Zn stress, the % of AMF root colonization was 25% on average,

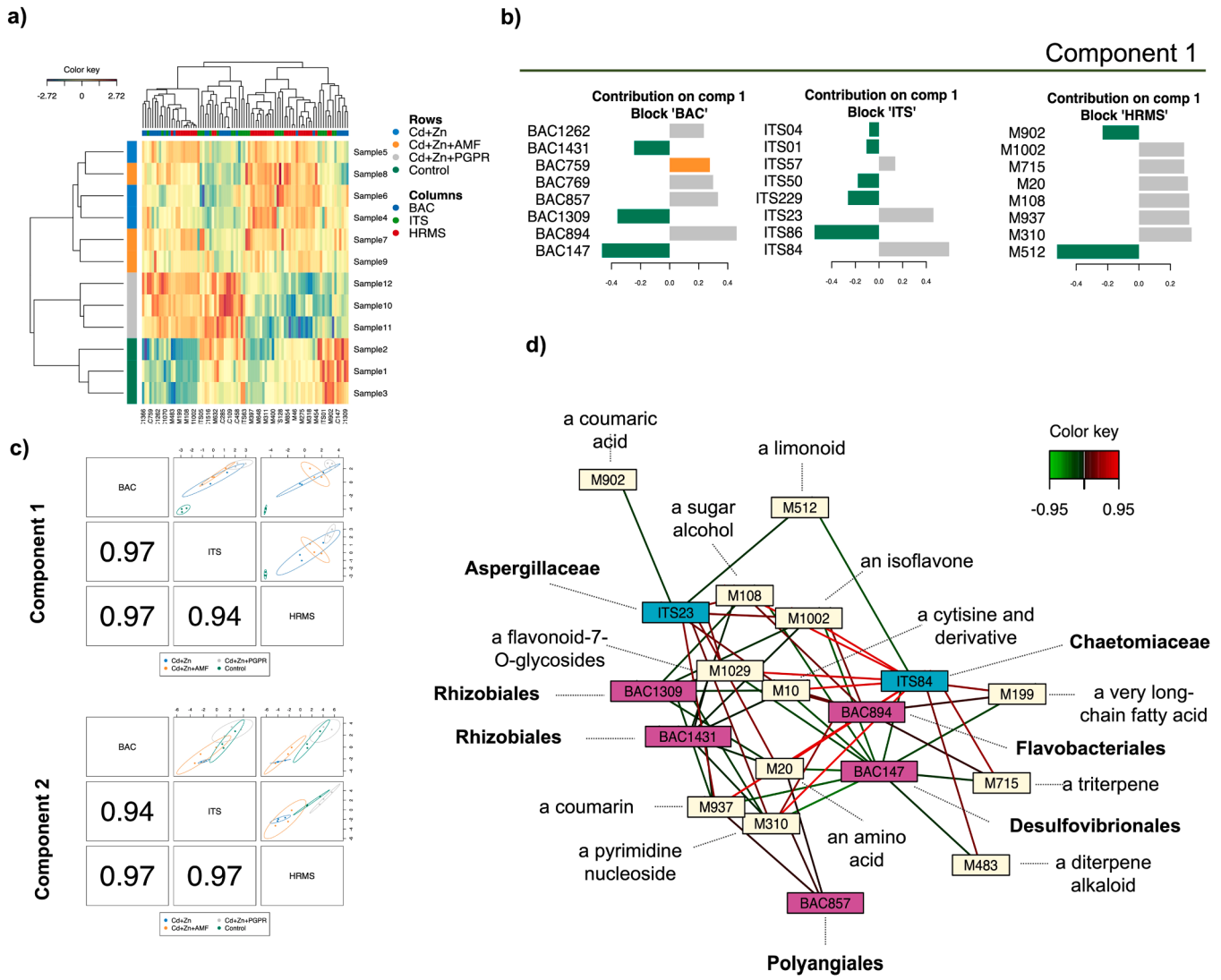

Fig. 7. DIABLO correlation analysis between root exudate profiles (HRMS), root bacterial (BAC) and fungal (ITS) endospheric microbial populations treated with untreated control, Cd+Zn, Cd+Zn+AMF, and Cd+Zn+PGPR in tomato plants. a) correlation heat map, b) loading features of the three datasets, c) correlation matrix for components 1 and 2, and d) network analysis of the most correlated features coming from the three datasets. Abbreviation: AMF = Arbuscular Mycorrhizae Fungi, PGPR = Plant Growth Promoting Rhizobacteria.

found to be lower than in either AMF alone or in single Cd or Zn exposure (when compared with our previous study by assessing their toxicity in single exposure), suggesting a synergistic effect when combined (L. Zhang et al., 2023). Another stress-adaptive mechanism involved stomatal closure, as reflected by increased RWC in Cd+Zn-treated plants, tissue hydration through reduced transpiration, growth inhibition, and osmotic adjustment, rather than improved physiological performance. In this context, the concomitant decrease in MSI indicates that cellular integrity was nonetheless impaired. Therefore, the higher RWC observed in Cd+Zn plants should not be interpreted as a lower stress condition, but rather as a stress-associated water balance response (Rucińska and Rucińska-Sobkowiak, 2016).

The competition between HMs and mineral nutrients for plant uptake and accumulation is a significant concern in metal-contaminated soils. This competition interferes with the proper assimilation and distribution of both essential and non-essential mineral elements by plants, resulting in imbalanced nutrient availability with consequences for plant growth and development (Pandey et al., 2022). Zn and Cd are divalent ions that may compete for binding sites on the root surface, and their combined use can induce both antagonistic and synergistic effects on several elements during plant uptake (Rizwan et al., 2019). In our study, the exposure of tomato plants to Cd+Zn induced a higher accumulation of both metals in roots than in leaves or fruits. In most plants, Cd sequestration in root vacuoles has been shown to reduce its transport through the xylem, resulting in limited translocation to leaves and fruits (Lux et al., 2011), while, conversely, a significant amount of Zn metal was translocated to the aerial organs, more notably in fruits under Cd+Zn+AMF treatment. Interestingly, Zn is an essential element; increased fruit Zn concentration does not necessarily indicate a food-safety risk. Nevertheless, since excessive chronic Zn intake can be detrimental to human health, the increase observed under AMF treatment highlights the need to evaluate consumer exposure and edible-tissue thresholds in future studies (Tolerable Upper Intake Levels for Vitamins and Minerals, 2006) (Overview on Tolerable Upper Intake Levels as Derived by the Scientific Committee on Food (SCF) and the EFSA Panel on Dietetic Products, Nutrition and Allergies (NDA), n.d.).

In the combined application of Cd+Zn, it has been reported that Zn might be the dominant factor affecting plant growth and nutrition at excess Zn levels, despite the Cd concentrations in plants (Rizwan et al., 2019). Notably, we observed a negative relationship between the accumulation of Cd, Zn, and Fe and MSI, indicating a close correlation with membrane stability imbalance. Excess Cd and Zn are known to

interfere with Fe homeostasis, leading to oxidative stress (Galaris et al., 2019; Y. Zhang et al., 2025). The results support the hypothesis that Fe dysregulation contributes to membrane damage under HM exposure. At the same time, Cd and, to a lesser extent, Zn showed positive correlations with root architectural traits (RSVD, RLD, RVD), suggesting that plants may respond to Cd exposure by enhancing root system development, as previously claimed (Farooq et al., 2022).

Usually, plant ion imbalance is associated with reduced physiological performance. Consistently, HMs have been increasingly reported to decrease net photosynthetic rates and water-use efficiency by inhibiting PSII activity and impairing thylakoid membranes (Riyazuddin et al., 2021). The decline in Fv/Fm and PI_{abs} in the Cd+Zn treatments was consistent with previous studies (Hidri et al., 2025). The reduced PSII activity induced by HMs has been reported to occur due to targeting multiple sites in chloroplast membranes, such as the D1 protein (Deng et al., 2013). Accordingly, reduced membrane stability in plants under Cd+Zn exposure could be due to disturbances in cell membrane permeability, followed by ionic imbalance, which is linked to decreased photosynthetic efficiency (Rai et al., 2016).

The mitigating effects of MBs on plant morphological and physiological indices reported contrasting tissue-specific effects, likely reflecting their distinct modes of action: PGPR primarily acts through phytohormone signaling and siderophore-mediated nutrient mobilization, whereas AMF enhances root development via hyphal networks that extend nutrient uptake capacity. This finding has been increasingly reported over recent years (L. Zhang et al., 2023). This observation was also supported by other studies, which reported that PGPR *Bacillus subtilis* increased plant growth and decreased Cd bioavailability, translocation, and uptake in ryegrass and wheat plants grown in Cd-contaminated soil (Ilyas et al., 2022; Q. Li et al., 2022). The higher membrane stability and lower ROS accumulation in plants treated with MBs helped alleviate oxidative damage under HM stress by modulating redox balance and strengthening antioxidant defenses, as previously reported by Omoarelojie et al. (2021). Moreover, the improved photosynthetic performance likely contributed to lower ROS production, probably by maintaining a more efficient electron transport chain that generates fewer harmful by-products during HMs toxicity (González et al., 2024).

AMF and PGPR differentially regulate metal detoxification and nutrient uptake in tomato plants

Under Cd+Zn stress, MBs differentially affected metal and nutrient allocation. Specifically, AMF significantly reduced the amount of Cd allocated in roots, while PGPR induced the most significant mitigation of Cd accumulation in all tomato organs. Translocation factor analysis further clarified these responses, showing that Cd was predominantly retained in roots (TF < 1), with an almost complete suppression of root-to-fruit transport under both AMF and PGPR treatments. This indicates that MBs mitigate Cd toxicity not only by reducing uptake, but also by restricting its long-distance translocation to aerial and edible tissues, likely through enhanced root retention and sequestration processes (Khanna et al., 2019; Kuang et al., 2023). Consistently, BCF values confirmed Cd retention in roots and negligible accumulation in fruits under microbial treatments.

The Zn translocation factor exhibited higher mobility, particularly under AMF, thereby promoting its allocation to fruits. This behavior supports a selective regulation of metal partitioning, where essential elements such as Zn remain mobile to sustain physiological functions, while toxic elements such as Cd are immobilized. This outcome was confirmed by You et al. (2021), highlighting a concentration-dependent pattern. By contrast, PGPR appeared more effective in alleviating Zn toxicity at the whole-plant level, likely reducing Zn uptake and then reducing excessive translocation to aerial tissues. This detoxification strategy may depend on interactions among the host plant, the microbial strain, the type of HM, and the ability to immobilize HM in the roots (Khanna et al., 2019). Notably, although AMF colonization was directly quantified at the end of the trial, PGPR persistence was not assessed using strain-specific approaches. Therefore, the observed PGPR-related responses should be interpreted as treatment-associated effects rather than direct evidence of stable establishment of *Pseudomonas* sp. So_08 in the rhizosphere.

The HMs and the MBs elicited differential effects in the uptake and allocation of macro- and micronutrients. Particularly, an increased accumulation of Ca and P was observed in the roots of tomato plants exposed to Cd+Zn stress, reflecting a broader reorganization of nutrient homeostasis under metal exposure (Hédiji et al., 2015). Nonetheless, differential responses were triggered by each biostimulant. Although AMF induced notable root uptake of micronutrients, including P, K, and Mg, the PGPR inoculation elicited remarkable responses in most micronutrients, reducing their uptake to levels comparable to those of control plants (Lau et al., 2022; L. Zhang et al., 2023). In this context, inoculation with AMF has been extensively reported to alleviate HM stress in soil by boosting P uptake via extraradical hyphae (Adeyemi et al., 2021). On the other hand, reports on the effects of PGPR on plant mineral absorption under HM toxicity can be contradictory. In some findings, PGPR increased plant uptake of elements such as Fe, P, Zn, and Mg (Pii et al., 2016), whereas in others, decreased uptake was reported (Khan et al., 2018; Tsegaye et al., 2022). Hence, PGPR may elicit mechanisms in response to the plant's needs to meet balanced nutrient requirements.

Microbial biostimulants reshape root exudation and influence rhizosphere microbial composition and activity under Cd+Zn stress

The exudate profile of tomato roots exposed to Cd+Zn alone led to a general induction of stress response mechanisms, characterized by reallocation of resources, highlighted by the reduced secretion of amino acids, nitrogen-containing compounds, and sugars, and by the activation of the antioxidant defense system, as evidenced by the increased exudation of phenolic compounds (e.g., syringic acid, xanthohumol, and chlorogenic acid). Notably, chlorogenic acid has also been reported to exhibit metal-chelating activity, particularly toward cations such as Zn and Cd (Kalinowska et al., 2020), a mechanism that contributes to metal tolerance and detoxification by modulating HM bioavailability and toxicity (Anjum et al., 2015). In addition, Cd+Zn exposure promoted the selective accumulation of coumarins (e.g., di-*O*-methylfraxetin), whose accumulation and secretion are well-documented responses to Fe deficiency, a condition frequently induced by excess Cd and Zn, as previously discussed (Sisó-Terraza et al., 2016; Y. Zhang et al., 2025).

Interestingly, both AMF and PGPR applications reshaped root exudate metabolism and influenced rhizosphere community composition. The absence of significant differences in β-diversity indicates that the overall rhizosphere community structure remained relatively stable across treatments. However, the enrichment of specific taxa detected by LEfSe, together with the DIABLO-based correlations between microbial features and root exudate metabolites, suggests a more targeted response. Specifically, PICRUSt2 analysis predicted the functional potential of the bacterial rhizosphere community by reporting the abundance of catechol degradation, aerobic toluene degradation, and aromatic compound cleavage pathways under Cd+Zn+AMF treatment, which indicates an increased potential for aromatic substrate turnover. This pattern is consistent with the root exudate data, in which Cd+Zn stress and microbial treatments altered phenolic and coumarin-like metabolites, and with the enrichment of *Bacillus* and *Flavobacterium*, taxa often associated with degradation of aromatic or complex plant-derived substrates and rhizosphere carbon cycling (Arora, 2020; Máté et al., 2022). By contrast, the strongest predicted response was an increase in starch degradation under Cd+Zn+PGPR treatment, suggesting enhanced bacterial potential for carbohydrate turnover, possibly linked to PGPR-induced changes in root carbon release. These patterns support the hypothesis that treatment-induced changes in root exudation may

contribute to the selective recruitment or stimulation of specific microbial taxa. Nevertheless, these associations should be interpreted cautiously, as the present data are correlative and do not prove direct contribution to stress mitigation by supporting exudate processing, nutrient cycling, and rhizosphere metabolic activity.

To provide a more integrated interpretation of these responses, a conceptual graph (Fig. 8) was developed to summarize the complementary mechanisms.

AMF-driven metabolic reprogramming enhances stress tolerance and beneficial bacterial recruitment

Treatment with AMF under Cd+Zn exposure led to a broad accumulation of most metabolite classes compared to the untreated control, suggesting its potential metabolic reprogramming activity under HM stress. This metabolic enhancement is consistent with the well-established ability of AMF to improve nutrient acquisition, reduce metal toxicity through sequestration or compartmentalization, and restore both primary and secondary metabolic pathways (W. Li et al., 2023; Y. Zhang et al., 2025). The accumulation of pyridoxine, tanshinone IIA, and sinapine, suggests a metabolic adjustment aimed at enhancing stress protection in inoculated plants, since they are associated with antioxidant activity, metal chelation, membrane-protective, and redox-modulatory properties (Denslow et al., 2005; Kim et al., 2023; Yates et al., 2019). Notably, tanshinone IIA has been reported to activate protective mechanisms in AMF-colonized plants (Wu et al., 2021), and the decrease in biotin levels may indicate increased utilization of biotin in fatty acid synthesis and energy metabolism to support the fungal symbiont (Wang et al., 2020). Overall, these classes of exudated molecules could influence the rhizosphere microbiome, serving as nutrients and signals for microbes, highlighting the complex biochemical strategies promoted by AMF to enhance plant resilience under Cd+Zn stress (Samsatly et al., 2020).

In line with this metabolic shift, AMF-treated rhizospheres exhibited an increased relative abundance of Bacillaceae, well known for their tolerance to HMs and their ability to produce siderophores, organic acids, and antioxidants that contribute to metal immobilization, detoxification, and stress alleviation in contaminated soils (Alves et al., 2022). Previous studies have reported that *Caulobacter* populations can be severely depleted in high-Cd environments (Salam et al., 2020), a pattern observed in our experiment. Several *Caulobacter* strains have been associated with beneficial plant-interactions and reported to exhibit plant growth–promoting activities (Wilhelm, 2018; Yang et al., 2019). Notably, the addition of AMF restored and even increased the abundance of this genus compared to combined stress and control conditions.

AMF treatment also increased the relative abundance of Flavobacteriales to levels similar with the control, suggesting a partial restoration of bacterial groups potentially impaired by HM stress. Members of this order are commonly associated with organic matter mineralization and nutrient cycling and may also contribute to metal detoxification through active transport, extracellular and intracellular sequestration, and metal transformation or reduction processes (Joshi et al., 2023; Ling et al., 2022). These results suggest that AMF-driven metabolic reprogramming not only enhances plant stress tolerance but

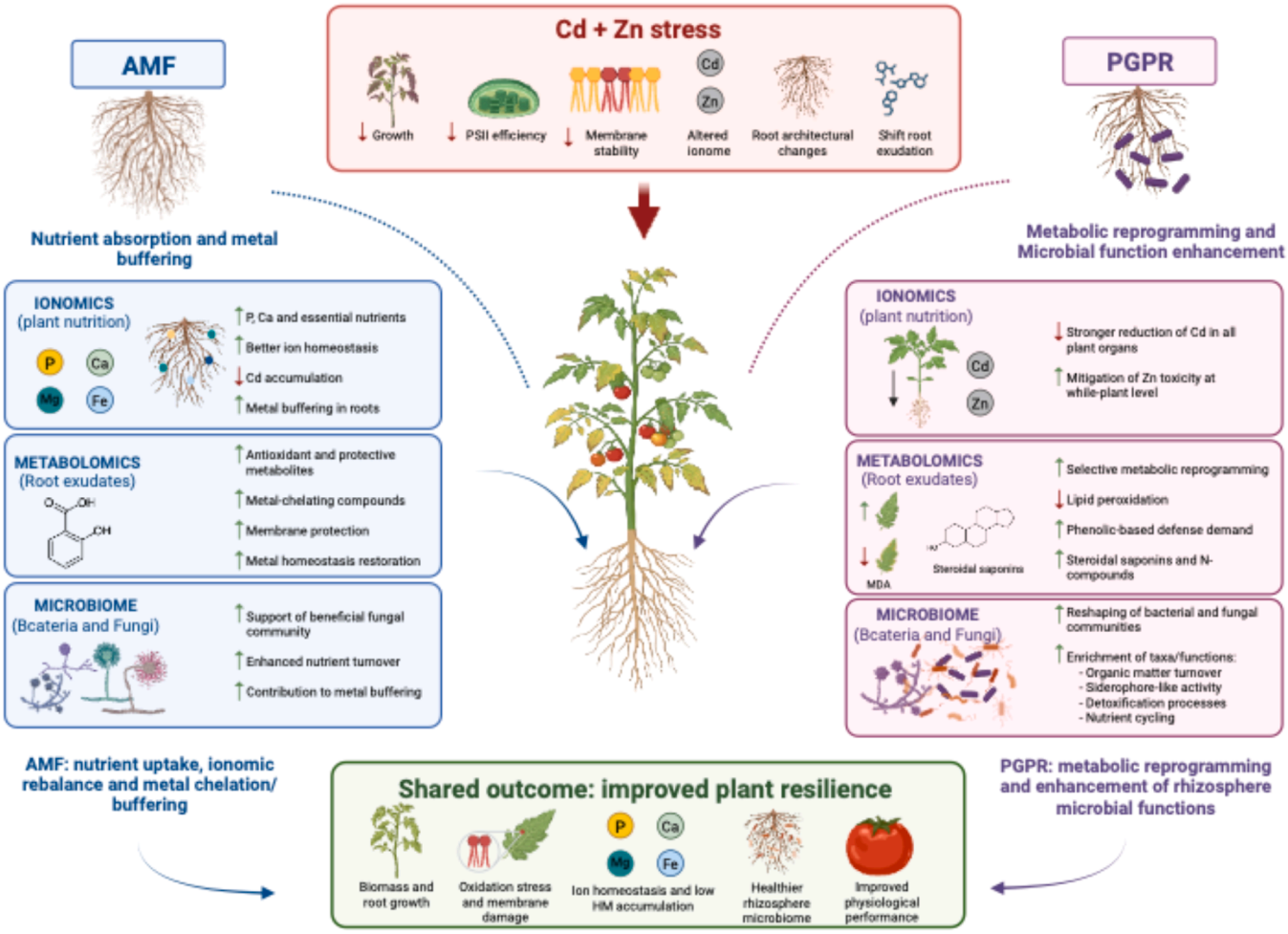

Fig. 8. Integrated conceptual model summarizing the complementary mitigation mechanisms triggered by AMF and PGPR in tomato plants exposed to combined Cd+Zn stress.

also favors the recruitment of bacterial taxa functionally adapted to nutrient turnover and metal-stressed rhizosphere environments.

PGPR-induced exudate modulation supports detoxification and rhizosphere functional diversification

The treatment with PGPR under Cd+Zn exposure showed a more complex metabolic response than the AMF, reporting both up- and down-regulated metabolites. Specifically, lipid-related metabolites (e.g., ricinoleic, stearic, and pentacosanoic acids) and phenylpropanoids were down-regulated under PGPR inoculation. A decreased turnover of lipids under HM stress could be associated with reduced lipid peroxidation due to PGPR protection (Khan et al., 2019). Similarly, the decrease in phenolic compounds suggests that the treatment may alleviate the need for phenolic-based defenses, likely by activating alternative stress-mitigation pathways, such as siderophore production, as previously demonstrated for this PGPR *Pseudomonas* sp. strain So_08 (L. Zhang et al., 2023), or accumulation of steroidal saponins such as polyphyllin VI, well-known for their allelopathic function against microbial pathogens (Gao et al., 2022). Notably, Nakayasu et al. (2021) reported that the accumulation of steroidal saponins in the rhizosphere could alter bacterial communities, with the magnitude of alteration varying in a molecule-dependent manner (Nakayasu et al., 2021). Accordingly, we observed an increase in both bacterial and fungal populations under Cd+Zn+PGPR treatment. The multiomics data integration highlighted an enrichment of the fungal families Aspergillaceae (i.e., *Penicillium* genus) and Chaetomiaceae (i.e., *Corynascella* genus), which are strictly and positively correlated with several exudate metabolites, including sugars, amino acids, phenolic compounds, terpenoids, and lipids, suggesting that PGPR-induced modulation creates a niche that favors these fungal families, which in turn may contribute to stress mitigation by enhancing organic matter decomposition around the roots (Gupta et al., 2022). Specifically, Aspergillaceae are fungi capable of degrading complex organic substrates through the production and secretion of a wide range of extracellular enzymes, such as cellulases, xylanases, pectinases, and lipases, to hydrolyze plant biomass, oils, and other complex carbon sources, thereby acting as key components of nutrient cycling (Rosas-Vega et al., 2025; Saleh et al., 2021). In HM-contaminated soils, this family could assist in metal tolerance mechanisms by producing siderophore-like compounds that can chelate metals, influence metal speciation, and nutrient availability (Happacher et al., 2023). Likewise, Chaetomiaceae, specifically the *Corynascella* genus, is a root endophytic fungus reported by Xiang et al. (2025) to have plant growth-promoting activity under low-nutrient conditions and systemic resistance against plant pathogens (Xiang et al., 2025). Their positive association with root-derived sugars and amino acids is consistent with these fungi's plant growth-promoting capacity, while correlations with phenolics and terpenoids suggest their potential active participation in the plant defense system and their role in mediating signaling within the rhizosphere.

The same effect was observed for bacterial families, where PGPR treatment under Cd+Zn stress was associated with increased abundance of *Geobacter* and *Bacillus*, taxa commonly linked to metal detoxification through redox transformations, metal immobilization, and the production of chelating and antioxidative compounds. These shifts suggest that PGPR inoculation promotes a rhizosphere community with complementary functions in detoxification and carbon cycling, which may indirectly support plant growth and stress tolerance under HM conditions.

Conclusions

This study demonstrates that Cd+Zn co-contamination severely compromises tomato growth by altering nutrient uptake, impairing photosynthetic efficiency, and destabilizing cellular membranes. Plants responded by modifying root system architecture and reprogramming root exudation toward defense-related metabolites, including phenolics and coumarins linked to antioxidant activity and Fe mobilization. Microbial biostimulants significantly mitigated these detrimental effects, although through distinct mechanisms. AMF primarily enhanced nutrient acquisition, restored metabolic homeostasis, and promoted the accumulation of protective metabolites with antioxidant and metal-chelating properties. PGPR induced a more selective metabolic adjustment, reducing lipid peroxidation and phenolic-based defenses while stimulating the production of steroidal saponins and nitrogen-containing compounds. Importantly, PGPR selectively influenced rhizosphere microbial taxa, enriching fungi and bacteria capable of degrading complex organic matter, producing siderophore-like compounds, and contributing to HM detoxification. Together, these findings highlight the complementary roles of AMF and PGPR in modulating plant physiology, metabolism, and microbiome composition, offering promising strategies for enhancing crop resilience in HM-contaminated soils. These results should be interpreted as proof-of-concept evidence obtained under controlled pot conditions, and further field-scale validation is needed before agronomic translation. Pot experiments cannot fully reproduce the complexity of field environments, including soil heterogeneity, climate variability, and interactions with native microbial communities, all of which may strongly influence inoculant establishment and plant responses, as well as multi-variety validation and long-term field experiment for robustness and reproducibility prospective should be considered. In this context, practical implementation may be influenced by inoculant shelf-life stability, soil-dependent performance, and competition with native microbial communities. While the AMF used here is already available as a commercial formulation, the translation of the PGPR-based approach would benefit from improved formulation strategies, such as encapsulated or carrier-based inoculants designed to enhance cell survival, storage stability, and controlled release. Furthermore, a relevant future perspective will be to investigate the combined application of the two biostimulants, with the aim of assessing potential additive or synergistic effects under HM stress conditions.

Data availability

The data are provided upon request and in the supplementary material.

Funding

This research received no specific grant from funding agencies in the public, commercial, or not-for-profit sectors.

Supplementary data

Figure. S1: Root morphology analysis; Figure. S2: AMF colonization; Figure. S3: Spearman correlation heatmap; Figure. S4: hierarchical cluster analysis and Partial Least Squares Discriminant Analysis; Figure. S5: PICRUSt2; Table S1: Ionomic analysis; Table S2: Bioconcentration factor (BCF) of Cd and Zn; Table S3: Dataset exudate profile; Table S4: VIP markers from OPLS-DA models; Table S5: different α-diversity indices; Table S6: DIABLO loading features.

CRediT authorship contribution statement

Leilei Zhang: Writing – original draft, Validation, Supervision, Software, Investigation, Formal analysis, Data curation, Conceptualization. **Monica Yorlady Alzate Zuluaga:** Writing – original draft, Validation, Software, Methodology, Formal analysis, Data curation. **Gabriele Bellotti:** Writing – original draft, Validation, Software, Methodology, Formal analysis, Data curation. **Hajar Salehi:** Writing – original draft, Validation, Software, Formal analysis, Data curation. **Angelica Barone:** Validation, Software, Methodology, Formal analysis, Data curation. **Filippo Vaccari:** Software, Formal analysis, Data curation. **Stefano Amaducci:** Writing – review & editing, Supervision, Resources, Data curation. **Youry Pii:** Writing – review & editing,

Supervision, Resources, Data curation. **Edoardo Puglisi:** Writing – review & editing, Supervision, Resources, Methodology, Data curation. **Luigi Lucini:** Writing – review & editing, Supervision, Resources, Data curation, Conceptualization.

Declaration of competing interest

The authors declare that they have no known competing financial interests or personal relationships that could have appeared to influence the work reported in this paper.

Acknowledgments

The authors thank the "Romeo ed Enrica Invernizzi" foundation (Milan, Italy) for its kind support of the metabolomics facility at Università Cattolica del Sacro Cuore.

Supplementary materials

Supplementary material associated with this article can be found, in the online version, at doi:10.1016/j.stress.2026.101434.

References

Adeyemi, N.O., Atayese, M.O., Sakariyawo, O.S., Azeez, J.O., Abayomi Sobowale, S.P., Olubode, A., Mudathir, R., Adebayo, R., Adeoye, S., 2021. Alleviation of heavy metal stress by arbuscular mycorrhizal symbiosis in glycine max (L.) grown in copper, lead and zinc contaminated soils. Rhizosphere 18, 100325. https://doi.org/10.1016/J.RHISPH.2021.100325.

Alengebawy, A., Abdelkhalek, S.T., Qureshi, S.R., Wang, M.Q., 2021. Heavy metals and pesticides toxicity in agricultural soil and plants: ecological risks and Human health implications. Toxics 9 (3), 42. https://doi.org/10.3390/TOXICS9030042. *Vol. 9, Page 42*.

Alves, A.R.A., Yin, Q., Oliveira, R.S., Silva, E.F., Novo, L.A.B., 2022. Plant growth-promoting bacteria in phytoremediation of metal-polluted soils: current knowledge and future directions. Sci. Total Environ. 838, 156435. https://doi.org/10.1016/J.SCITOTENV.2022.156435.

Angulo-Bejarano, P.I., Puente-Rivera, J., Cruz-Ortega, R., 2021. Metal and metalloid toxicity in plants: an overview on molecular aspects. Plants 10 (4), 635. https://doi.org/10.3390/PLANTS10040635. *Vol. 10, Page 635*.

Anjum, N.A., Hasanuzzaman, M., Hossain, M.A., Thangavel, P., Roychoudhury, A., Gill, S.S., Merlos Rodrigo, M.A., Adam, V., Fujita, M., Kizek, R., Duarte, A.C., Pereira, E., Ahmad, I., 2015. Jacks of metal/metalloid chelation trade in plants—an overview. Front. Plant Sci. 6, 124587. https://doi.org/10.3389/FPLS.2015.00192/XML. APR.

Araniti, F., Miras-Moreno, B., Lucini, L., Landi, M., Abenavoli, M.R., 2020. Metabolomic, proteomic and physiological insights into the potential mode of action of thymol, a phytotoxic natural monoterpenoid phenol: the phytotoxic effect of thymol on adult plants of A. thaliana. Plant Physiol. Biochem. 153, 141–153. https://doi.org/10.1016/j.plaphy.2020.05.008. May.

Arora, P.K., 2020. Bacilli-mediated degradation of xenobiotic compounds and heavy metals. Front. Bioeng. Biotechnol. 8, 570307. https://doi.org/10.3389/FBIOE.2020.570307/XML.

Balali-Mood, M., Naseri, K., Tahergorabi, Z., Khazdair, M.R., Sadeghi, M., 2021. Toxic mechanisms of five heavy metals: mercury, lead, chromium, cadmium, and arsenic. Front. Pharmacol. 12, 643972. https://doi.org/10.3389/FPHAR.2021.643972/XML.

Bonini, P., Rouphael, Y., Miras-Moreno, B., Lee, B., Cardarelli, M., Erice, G., Cirino, V., Lucini, L., Colla, G., 2020. A microbial-based biostimulant enhances sweet Pepper performance by metabolic reprogramming of phytohormone profile and secondary metabolism. Front. Plant Sci. 11, 567388. https://doi.org/10.3389/FPLS.2020.567388/BIBTEX.

Caspi, R., Billington, R., Ferrer, L., Foerster, H., Fulcher, C.A., Keseler, I.M., Kothari, A., Krummenacker, M., Latendresse, M., Mueller, L.A., Ong, Q., Paley, S., Subhraveti, P., Weaver, D.S., Karp, P.D., 2016. The MetaCyc database of metabolic pathways and enzymes and the BioCyc collection of pathway/genome databases. Nucleic. Acids. Res. 44 (D1), D471–D480. https://doi.org/10.1093/NAR/GKV1164.

Chen, D., Saeed, M., Ali, M.N.H.A., Raheel, M., Ashraf, W., Hassan, Z., Hassan, M.Z., Farooq, U., Hakim, M.F., Rao, M.J., Naqvi, S.A.H., Moustafa, M., Al-Shehri, M., Negm, S., 2023. Plant growth promoting rhizobacteria (PGPR) and arbuscular mycorrhizal fungi combined application reveals enhanced soil fertility and rice production. Agronomy 13 (2), 550. https://doi.org/10.3390/AGRONOMY13020550. *2023, Vol. 13, Page 550*.

Chong, J., Liu, P., Zhou, G., Xia, J., 2020. Using MicrobiomeAnalyst for comprehensive statistical, functional, and meta-analysis of microbiome data. Nat. Protoc. 15 (3), 799–821. https://doi.org/10.1038/s41596-019-0264-1.

Deng, C., Zhang, D., Pan, X., Chang, F., Wang, S., 2013. Toxic effects of mercury on PSI and PSII activities, membrane potential and transthylakoid proton gradient in microsorium pteropus. J. Photochem. Photobiol. B, Biol. 127, 1–7. https://doi.org/10.1016/J.JPHOTOBIOL.2013.07.012.

Denslow, S.A., Walls, A.A., Daub, M.E., 2005. Regulation of biosynthetic genes and antioxidant properties of vitamin B6 vitamers during plant defense responses. Physiol. Mol. Plant Pathol. 66 (6), 244–255. https://doi.org/10.1016/J.PMPP.2005.09.004.

Douglas, G.M., Maffei, V.J., Zaneveld, J.R., Yurgel, S.N., Brown, J.R., Taylor, C.M., Huttenhower, C., Langille, M.G.I., 2020. PICRUSt2 for prediction of metagenome functions. Nat. Biotechnol. 38 (6), 685–688. https://doi.org/10.1038/S41587-020-0548-6.

Dutta, S., Mitra, M., Agarwal, P., Mahapatra, K., De, S., Sett, U., Roy, S., 2018. Oxidative and genotoxic damages in plants in response to heavy metal stress and maintenance of genome stability. Plant Signal. Behav. (8), 1–49. https://doi.org/10.1080/15592324.2018.1460048.

Estaki, M., Jiang, L., Bokulich, N.A., McDonald, D., González, A., Kosciolek, T., Martino, C., Zhu, Q., Birmingham, A., Vázquez-Baeza, Y., Dillon, M.R., Bolyen, E., Caporaso, J.G., Knight, R., 2020. QIIME 2 enables comprehensive end-to-end analysis of diverse microbiome data and comparative studies with publicly available data. Curr. Protoc. Bioinformatics. 70 (1). https://doi.org/10.1002/CPBI.100.

Farooq, T.H., Rafay, M., Basit, H., Shakoor, A., Shabbir, R., Riaz, M.U., Ali, B., Kumar, U., Qureshi, K.A., Jaremko, M., 2022. Morpho-physiological growth performance and phytoremediation capabilities of selected xerophyte grass species toward Cr and Pb stress. Front. Plant Sci. 13, 997120. https://doi.org/10.3389/FPLS.2022.997120/BIBTEX.

Galanova, O.O., Mitkin, N.A., Danilova, A.A., Pavshintsev, V.V., Tsybizov, D.A., Zakharenko, A.M., Golokhvast, K.S., Grigoryeva, T.V., Markelova, M.I., Vatlin, A.A., 2025. Assessment of soil health through metagenomic analysis of bacterial diversity in Russian black soil. Microorganisms 13 (4), 854. https://doi.org/10.3390/MICROORGANISMS13040854/S1.

Galaris, D., Barbouti, A., Pantopoulos, K., 2019. Iron homeostasis and oxidative stress: an intimate relationship. Biochim. Biophys. Acta BBA - Mol. Cell Res. 1866 (12), 118535. https://doi.org/10.1016/J.BBAMCR.2019.118535.

Gao, X., Su, Q., Li, J., Yang, W., Yao, B., Guo, J., Li, S., Liu, C., 2022. RNA-seq analysis reveals the important co-expressed genes associated with polyphyllin biosynthesis during the developmental stages of Paris polyphylla. BMC. Genomics. 23 (Suppl 1), 559. https://doi.org/10.1186/S12864-022-08792-2.

Gaur, V.K., Sharma, P., Gaur, P., Varjani, S., Ngo, H.H., Guo, W., Chaturvedi, P., Singhania, R.R., 2021. Sustainable mitigation of heavy metals from effluents: toxicity and fate with recent technological advancements. Bioengineered 12 (1), 7297–7313. https://doi.org/10.1080/21655979.2021.1978616.

González, M.C., Roitsch, T., Pandey, C., 2024. Antioxidant responses and redox regulation within plant-beneficial microbe interaction. Antioxidants 13 (12), 1553. https://doi.org/10.3390/ANTIOX13121553. *2024, Vol. 13, Page 1553*.

Guo, J., Guo, Y., Yang, J., Yang, J., Zheng, G., Chen, T., Li, Z., Wang, X., Bian, J., Meng, X., 2020. Effects and interactions of cadmium and zinc on root morphology and metal translocation in two populations of hylotelephium spectabile (Boreau) H. Ohba, a potential Cd-accumulating species. Environ. Sci. Pollut. Res. 27 (17), 21364–21375. https://doi.org/10.1007/S11356-020-08660-0/FIGURES/5.

Gupta, S., Singh, U.B., Kumar, A., Ramtekey, V., Jayaswal, D., Singh, A.N., Sahni, P., & Kumar, S. (2022). *Role of rhizosphere microorganisms in endorsing overall plant growth and development*. 323–353. https://doi.org/10.1007/978-981-19-4101-6_16.

Happacher, I., Aguiar, M., Yap, A., Decristoforo, C., Haas, H., 2023. Fungal siderophore metabolism with a focus on Aspergillus fumigatus: impact on biotic interactions and potential translational applications. Essays Biochem. 67 (5), 829–842. https://doi.org/10.1042/EBC20220252.

Hédiji, H., Djebali, W., Belkadhi, A., Cabasson, C., Moing, A., Rolin, D., Brouquisse, R., Gallusci, P., Chaïbi, W., 2015. Impact of long-term cadmium exposure on mineral content of solanum lycopersicum plants: consequences on fruit production. S. Afr. J. Bot. 97, 176–181. https://doi.org/10.1016/J.SAJB.2015.01.010.

Hidri, R., Azri, R., Burow, K., Zorrig, W., Debez, A., Alyami, N.M., Rabhi, M., Bensalem-Fnayou, A., Mliki, A., Franken, P., Aroca, R., 2025. Significance of photosystem integrity and reducing Cd accumulation in mitigating Cd stress on olive tree inoculated with soil-borne bacteria consortium is variety-dependent. Plant Stress. 15, 100788. https://doi.org/10.1016/J.STRESS.2025.100788.

Ilyas, N., Akhtar, N., Yasmin, H., Sahreen, S., Hasnain, Z., Kaushik, P., Ahmad, A., Ahmad, P., 2022. Efficacy of citric acid chelate and Bacillus sp. in amelioration of cadmium and chromium toxicity in wheat. Chemosphere 290, 133342. https://doi.org/10.1016/J.CHEMOSPHERE.2021.133342.

Jarin, A.S., Khan, M.A.R., Apon, T.A., Islam, M.A., Rahat, A., Akter, M., Anik, T.R., Nguyen, H.M., Nguyen, T.T., Ha, C.V., Tran, L.S.P., 2025. Plant responses to heavy metal stresses: mechanisms, defense strategies, and nanoparticle-assisted remediation. Plants 14 (24), 3834. https://doi.org/10.3390/PLANTS14243834. *2025, Vol. 14*.

Joshi, S., Gangola, S., Bhandari, G., Bhandari, N.S., Nainwal, D., Rani, A., Malik, S., Slama, P., 2023. Rhizospheric bacteria: the key to sustainable heavy metal detoxification strategies. Front. Microbiol. 14, 1229828. https://doi.org/10.3389/FMICB.2023.1229828/XML.

Kalinowska, M., Sienkiewicz-Gromiuk, J., Świderski, G., Pietryczuk, A., Cudowski, A., Lewandowski, W., 2020. Zn(II) complex of plant phenolic chlorogenic acid: antioxidant, antimicrobial and structural studies. Materials 13 (17), 3745. https://doi.org/10.3390/MA13173745.

Kaushal, P., Pati, A.M., 2025. Unleashing rhizobacteria for sustainable soil remediation: PGPR roles in heavy metal tolerance, detoxification, and plant productivity. Front. Microbiol. 16, 1662000. https://doi.org/10.3389/FMICB.2025.1662000/ENDNOTE.

Khan, N., Bano, A., Rahman, M.A., Guo, J., Kang, Z., Babar, M.A., 2019. Comparative physiological and metabolic analysis reveals a complex mechanism involved in

drought tolerance in Chickpea (Cicer arietinum L.) induced by PGPR and PGRs. Sci. Rep. 9 (1), 2097. https://doi.org/10.1038/S41598-019-38702-8.
Khan, N., Zandi, P., Ali, S., Mehmood, A., Shahid, M.A., 2018. Impact of salicylic acid and PGPR on the drought tolerance and phytoremediation potential of helianthus annus. Front. Microbiol. 9, 413204. https://doi.org/10.3389/FMICB.2018.02507/BIBTEX. OCT.
Khanna, K., Jamwal, V.L., Gandhi, S.G., Ohri, P., Bhardwaj, R., 2019. Metal resistant PGPR lowered Cd uptake and expression of metal transporter genes with improved growth and photosynthetic pigments in Lycopersicon esculentum under metal toxicity. Sci. Rep. 9 (1), 5855. https://doi.org/10.1038/s41598-019-41899-3. *2019 9:1*.
Kim, D.G., Ryu, J., Yang, B., Lee, Y.J., Kim, J.H., Kim, J., Kim, W.J., Kim, S.H., Kwon, S. J., Kim, J.B., Kang, S.Y., Lyu, J.I.L., Bae, C.H., Ahn, J.W., 2023. Genetic variation and association analysis of phenolic compounds in rapeseed (Brassica napus L.) mutant lines using genotyping-by-sequencing (GBS). Horticulturae 9 (11), 1204. https://doi.org/10.3390/HORTICULTURAE9111204/S1.
R. Kiran, B., Sharma, R., 2022. Effect of heavy metals: an overview Mater. Today: Proc. 51, 880–885. https://doi.org/10.1016/J.MATPR.2021.06.278.
Kong, Z., Liu, H., 2022. Modification of rhizosphere microbial communities: a possible mechanism of plant growth promoting rhizobacteria enhancing plant growth and fitness. Front. Plant Sci. 13, 920813. https://doi.org/10.3389/FPLS.2022.920813/TEXT.
Kuang, Y., Li, X., Wang, Z., Wang, X., Wei, H., Chen, H., Hu, W., Tang, M., 2023. Effects of arbuscular mycorrhizal fungi on the growth and root cell ultrastructure of eucalyptus grandis under Cadmium stress. J. Fungi 9 (2), 140. https://doi.org/10.3390/JOF9020140. *2023, Vol. 9*.
Lanier, C., Bernard, F., Dumez, S., Leclercq-Dransart, J., Lemière, S., Vandenbulcke, F., Nesslany, F., Platel, A., Devred, I., Hayet, A., Cuny, D., Deram, A., 2019. Combined toxic effects and DNA damage to two plant species exposed to binary metal mixtures (Cd/Pb). Ecotoxicol. Environ. Saf. 167, 278–287. https://doi.org/10.1016/J.ECOENV.2018.10.010.
Lau, S.E., Teo, W.F.A., Teoh, E.Y., Tan, B.C., 2022. Microbiome engineering and plant biostimulants for sustainable crop improvement and mitigation of biotic and abiotic stresses. Discov. Food 2 (1), 9. https://doi.org/10.1007/S44187-022-00009-5. *2022 2:1*.
Li, Q., Xing, Y., Huang, B., Chen, X., Ji, L., Fu, X., Li, T., Wang, J., Chen, G., Zhang, Q., 2022. Rhizospheric mechanisms of Bacillus subtilis bioaugmentation-assisted phytostabilization of cadmium-contaminated soil. Sci. Total. Environ. 825, 154136. https://doi.org/10.1016/J.SCITOTENV.2022.154136.
Li, W., Chen, K., Li, Q., Tang, Y., Jiang, Y., Su, Y., 2023. Effects of arbuscular mycorrhizal fungi on alleviating cadmium stress in Medicago truncatula Gaertn. Plants 12 (3), 547. https://doi.org/10.3390/PLANTS12030547.
Ling, N., Wang, T., Kuzyakov, Y., 2022. Rhizosphere bacteriome structure and functions. Nat. Commun. 13 (1), 836. https://doi.org/10.1038/s41467-022-28448-9. *2022 13:1*.
Lux, A., Martinka, M., Vaculík, M., White, P.J., 2011. Root responses to cadmium in the rhizosphere: a review. J. Exp. Bot. 62 (1), 21–37. https://doi.org/10.1093/JXB/ERQ281.
Martos, S., Ye, M., Riofrío, A., Tolrà, R., Bianucci, E., 2025. Enhancing peanut crop quality under arsenic stress through agronomic amendments. Agriculture 15 (21), 2300. https://doi.org/10.3390/AGRICULTURE15212300/S1.
Máté, R., Kutasi, J., Bata-Vidács, I., Kosztik, J., Kukolya, J., Tóth, E., Bóka, K., Táncsics, A., Kovács, G., Nagy, I., Tóth, Á., 2022. Flavobacterium hungaricum sp. nov. A novel soil inhabitant, cellulolytic bacterium isolated from plough field. Arch. Microbiol. 204 (6), 301. https://doi.org/10.1007/S00203-022-02905-X/FIGURES/1.
Mertens, J., & Smolders, E. (2013). *Zinc*. 465–493. https://doi.org/10.1007/978-94-007-4470-7_17.
Nakayasu, M., Yamazaki, S., Aoki, Y., Yazaki, K., Sugiyama, A., 2021. Triterpenoid and steroidal saponins differentially influence soil bacterial genera. Plants 10 (10), 2189. https://doi.org/10.3390/PLANTS10102189/S1.
Noor, I., Sohail, H., Sun, J., Nawaz, M.A., Li, G., Hasanuzzaman, M., Liu, J., 2022. Heavy metal and metalloid toxicity in horticultural plants: tolerance mechanism and remediation strategies. Chemosphere 303, 135196. https://doi.org/10.1016/J.CHEMOSPHERE.2022.135196.
Omoarelojie, L.O., Kulkarni, M.G., Finnie, J.F., Van Staden, J., 2021. Biostimulants and the modulation of plant antioxidant systems and properties. Biostimulants Crops Seed Germination Plant Dev.: Pract. Approach 333–363. https://doi.org/10.1016/B978-0-12-823048-0.00008-3.
Pandey, A.K., Zorić, L., Sun, T., Karanović, D., Fang, P., Borišev, M., Wu, X., Luković, J., Xu, P., 2022. The anatomical basis of heavy metal responses in legumes and their impact on plant–Rhizosphere interactions. Plants 11 (19), 2554. https://doi.org/10.3390/PLANTS11192554. *2022, Vol. 11, Page 2554*.
Pii, Y., Marastoni, L., Springeth, C., Fontanella, M.C., Beone, G.M., Cesco, S., Mimmo, T., 2016. Modulation of Fe acquisition process by Azospirillum brasilense in cucumber plants. Environ. Exp. Bot. 130, 216–225. https://doi.org/10.1016/J.ENVEXPBOT.2016.06.011.
Rai, R., Agrawal, M., Agrawal, S.B., 2016. Impact of heavy metals on physiological processes of plants: with special reference to photosynthetic system. Plant Responses Biot. 127–140. https://doi.org/10.1007/978-981-10-2860-1_6.
Rajapitamahuni, S., Kang, B.R., Lee, T.K., 2023. Exploring the roles of arbuscular mycorrhizal fungi in plant–Iron homeostasis. Agriculture 13 (10), 1918. https://doi.org/10.3390/AGRICULTURE13101918. *2023, Vol. 13, Page 1918*.
Rashid, A., Schutte, B.J., Ulery, A., Deyholos, M.K., Sanogo, S., Lehnhoff, E.A., Beck, L., 2023. Heavy metal contamination in agricultural soil: environmental pollutants affecting crop health. Agronomy 13 (6), 1521. https://doi.org/10.3390/AGRONOMY13061521/S1.
Rask, K.A., Johansen, J.L., Kjøller, R., Ekelund, F., 2019. Differences in arbuscular mycorrhizal colonisation influence cadmium uptake in plants. Environ. Exp. Bot. 162, 223–229. https://doi.org/10.1016/J.ENVEXPBOT.2019.02.022.
Riaz, M., Kamran, M., Fang, Y., Wang, Q., Cao, H., Yang, G., Deng, L., Wang, Y., Zhou, Y., Anastopoulos, I., Wang, X., 2021. Arbuscular mycorrhizal fungi-induced mitigation of heavy metal phytotoxicity in metal contaminated soils: a critical review. J. Hazard. Mater. 402, 123919. https://doi.org/10.1016/J.JHAZMAT.2020.123919.
Riyazuddin, R., Nisha, N., Ejaz, B., Khan, M.I.R., Kumar, M., Ramteke, P.W., Gupta, R., 2021. A comprehensive review on the heavy metal toxicity and sequestration in plants. Biomolecules 12 (1), 43. https://doi.org/10.3390/BIOM12010043. *2022, Vol. 12, Page 43*.
Rizwan, M., Ali, S., Rehman, M.Z., Maqbool, A., 2019. A critical review on the effects of zinc at toxic levels of cadmium in plants. Environ. Sci. Pollut. Res. 26 (7), 6279–6289. https://doi.org/10.1007/S11356-019-04174-6. *2019 26:7*.
Rosas-Vega, F.E., Pozzan, R., Martínez-Burgos, W.J., Letti, L.A.J., de Mattos, P.B.G., Ramos-Neyra, L.C., Spinillo Dudeque, G., Amaro Bittencourt, G., Dos S. Costa, G., Porto de Souza Vandenberghe, L., Soccol, C.R., 2025. Enzymes produced by the genus Aspergillus integrated into the biofuels industry using sustainable raw materials. Fermentation 11 (2), 62. https://doi.org/10.3390/FERMENTATION11020062. *2025, Vol. 11, Page 62*.
Rucińska, R., Rucińska-Sobkowiak, R., 2016. Water relations in plants subjected to heavy metal stresses. Acta Physiol. Plant. 38 (11), 257. https://doi.org/10.1007/S11738-016-2277-5. *2016 38:11*.
Sairam, R.K., Rao, K., Srivastava, G.C., 2002. Differential response of wheat genotypes to long term salinity stress in relation to oxidative stress, antioxidant activity and osmolyte concentration. Plant Sci. 163 (5), 1037–1046. https://doi.org/10.1016/S0168-9452(02)00278-9.
Salam, L.B., Obayori, O.S., Ilori, M.O., Amund, O.O., 2020. Effects of cadmium perturbation on the microbial community structure and heavy metal resistome of a tropical agricultural soil. Bioresour. Bioprocess. 7 (1), 25. https://doi.org/10.1186/S40643-020-00314-W. *2020 7:1*.
Saleh, H., Badierah, A.K., Redwan, R., El-Maradny, E.M., El-Fakharany, Y.A., El-Gendi, H., Saleh, A.K., Badierah, R., Redwan, E.M., El-Maradny, Y.A., El-Fakharany, E.M., 2021. A comprehensive insight into fungal enzymes: structure, classification, and their role in mankind's challenges. J. Fungi 8 (1), 23. https://doi.org/10.3390/JOF8010023. *Vol. 8, Page 23*.
Salek, R.M., Steinbeck, C., Viant, M.R., Goodacre, R., Dunn, W.B., 2013. The role of reporting standards for metabolite annotation and identification in metabolomic studies. Gigascience 2 (1), 13. https://doi.org/10.1186/2047-217X-2-13.
Samsatly, J., Bayen, S., Jabaji, S.H., 2020. Vitamin B6 is under a tight balance during disease development by rhizoctonia solani on different cultivars of potato and on Arabidopsis thaliana mutants. Front. Plant Sci. 11, 509412. https://doi.org/10.3389/FPLS.2020.00875/BIBTEX.
Sharafi, S., Salehi, F., 2025. Comprehensive assessment of heavy metal (HMs) contamination and associated health risks in agricultural soils and groundwater proximal to industrial sites. Sci. Rep. 15 (1), 7518. https://doi.org/10.1038/s41598-025-91453-7. *2025 15:1*.
Sisó-Terraza, P., Luis-Villarroya, A., Fourcroy, P., Briat, J.F., Abadía, A., Gaymard, F., Abadía, J., Álvarez-Fernández, A., 2016. Accumulation and secretion of coumarinolignans and other coumarins in Arabidopsis thaliana roots in response to iron deficiency at high pH. Front. Plant Sci. 7, 222572. https://doi.org/10.3389/FPLS.2016.01711/BIBTEX. NOVEMBER2016.
Sperdouli, I., 2022. Heavy metal toxicity effects on plants. Toxics 10 (12), 715. https://doi.org/10.3390/TOXICS10120715.
Syed, A., Elgorban, A.M., Bahkali, A.H., Eswaramoorthy, R., Iqbal, R.K., Danish, S., 2023. Metal-tolerant and siderophore producing Pseudomonas fluorescence and trichoderma spp. Improved the growth, biochemical features and yield attributes of chickpea by lowering Cd uptake. Sci. Rep. 13 (1), 4471. https://doi.org/10.1038/s41598-023-31330-3. *2023 13:1*.
Tamma, A.A., Lejcuś, K., Fiałkiewicz, W., Marczak, D., 2025. Advancing phytoremediation: a review of soil amendments for heavy metal contamination management. Sustainability 17 (13), 5688. https://doi.org/10.3390/SU17135688. *2025, Vol. 17, Page 5688*.
Tolerable upper intake levels for vitamins and minerals. (2006). European Food Safety Authority.
Tsegaye, Z., Alemu, T., Desta, F.A., Assefa, F., 2022. Plant growth-promoting rhizobacterial inoculation to improve growth, yield, and grain nutrient uptake of teff varieties. Front. Microbiol. 13, 896770. https://doi.org/10.3389/FMICB.2022.896770/BIBTEX.
van Dijk, J.R., Kranchev, M., Blust, R., Cuypers, A., Vissenberg, K., 2022. Arabidopsis root growth and development under metal exposure presented in an adverse outcome pathway framework. Plant Cell Environ. 45 (3), 737–750. https://doi.org/10.1111/PCE.14147.
Voglar, G.E., Leštan, D., 2010. Solidification/stabilisation of metals contaminated industrial soil from former Zn smelter in Celje, Slovenia, using cement as a hydraulic binder. J. Hazard. Mater. 178 (1–3), 926–933. https://doi.org/10.1016/J.JHAZMAT.2010.02.026.
Wang, Y., Wang, M., Ye, X., Liu, H., Takano, T., Tsugama, D., Liu, S., Bu, Y., 2020. Biotin plays an important role in Arabidopsis thaliana seedlings under carbonate stress. Plant Sci. 300, 110639. https://doi.org/10.1016/J.PLANTSCI.2020.110639.
Wilhelm, R.C., 2018. Following the terrestrial tracks of Caulobacter - redefining the ecology of a reputed aquatic oligotroph. ISME J. 12 (12), 3025–3037. https://doi.org/10.1038/s41396-018-0257-z. *2018 12:12*.

Wu, Y.H., Wang, H., Liu, M., Li, B., Chen, X., Ma, Y.T., Yan, Z.Y., 2021. Effects of native arbuscular mycorrhizae isolated on root biomass and secondary metabolites of salvia miltiorrhiza bge. Front. Plant Sci. 12, 617892. https://doi.org/10.3389/FPLS.2021.617892/BIBTEX.

Xiang, Z., Nakayashiki, H., Ikeda, K., 2025. Corynascella humicola, a root endophytic fungus from crabgrass, confers growth promotion and induced systemic resistance in gramineous plants. Biol. Control 207, 105810. https://doi.org/10.1016/J.BIOCONTROL.2025.105810.

Yang, E., Sun, L., Ding, X., Sun, D., Liu, J., Wang, W., 2019. Complete genome sequence of Caulobacter flavus RHGG3T, a type species of the genus Caulobacter with plant growth-promoting traits and heavy metal resistance. biotechnology 9 (2). https://doi.org/10.1007/S13205-019-1569-Z.

Yates, K., Pohl, F., Busch, M., Mozer, A., Watters, L., Shiryaev, A., Kong Thoo Lin, P., 2019. Determination of sinapine in rapeseed pomace extract: its antioxidant and acetylcholinesterase inhibition properties. Food Chem. 276, 768–775. https://doi.org/10.1016/J.FOODCHEM.2018.10.045.

You, Y., Wang, L., Ju, C., Wang, G., Ma, F., Wang, Y., Yang, D., 2021. Effects of arbuscular mycorrhizal fungi on the growth and toxic element uptake of phragmites australis (Cav.) trin. Ex steud under zinc/cadmium stress. Ecotoxicol. Environ. Saf. 213, 112023. https://doi.org/10.1016/J.ECOENV.2021.112023.

Zhang, L., Bellotti, G., Salehi, H., Puglisi, E., Lucini, L., 2025. Effects of arbuscular mycorrhizal fungi and metal-tolerant Pseudomonas fluorescens on mitigating cadmium and zinc stress in tomato. Plants 14 (21), 3353. https://doi.org/10.3390/PLANTS14213353.

Zhang, L., Zuluaga, M.Y.A., Pii, Y., Barone, A., Amaducci, S., Miras-Moreno, B., Martinelli, E., Bellotti, G., Trevisan, M., Puglisi, E., Lucini, L., 2023. A Pseudomonas plant growth promoting rhizobacterium and arbuscular mycorrhiza differentially modulate the growth, photosynthetic performance, nutrients allocation, and stress response mechanisms triggered by a mild Zinc and Cadmium stress in tomato. Plant Science 337, 111873. https://doi.org/10.1016/j.plantsci.2023.111873.